AIAA Guidance, Navigation and Control Conference and Exhibit
20 - 23 August 2007, Hilton Head, South Carolina

AIAA 2007-6409

Coordinated Path Following for Time-Critical Missions of Multiple UAVs via $\mathcal{L}_1$ Adaptive Output Feedback Controllers *

I. Kaminer, O. Yakimenko, V. Dobrokhodov, A. Pascoal,
N. Hovakimyan, C. Cao, A. Young, and V. Patel †

This paper develops a complete framework for coordinated control of multiple unmanned air vehicles (UAVs) that are tasked to execute collision-free maneuvers under strict spatial and temporal constraints in restricted airspace. The framework proposed includes strategies for deconflicted real-time path generation, nonlinear path following, and multiple vehicle coordination. Path following relies on the augmentation of existing autopilots with $\mathcal{L}_1$ adaptive output feedback control laws to obtain inner-outer loop control structures with guaranteed performance. Multiple vehicle coordination is achieved by enforcing temporal constraints on the speed profiles of the vehicles along their paths in response to information exchanged over a communication network. Again, $\mathcal{L}_1$ adaptive control is used to yield an inner-outer loop structure for vehicle coordination.

A rigorous proof of stability and performance bounds of the combined path following and coordination strategies is given. Flight test results obtained at Camp Roberts, CA in 2007 demonstrate the benefits of using $\mathcal{L}_1$ adaptive control for path following of a single vehicle. Hardware-in-the-loop simulations for two vehicles are discussed and provide a proof of concept for time-critical coordination of multiple vehicles over communication networks with fixed topologies.

I. Introduction

Autonomous systems are ubiquitous in both military and civilian applications. Among such systems, unmanned aerial vehicles (UAVs) play an important role and are widely used for military reconnaissance and strike operations, border patrol missions, forest fire detection, police surveillance and recovery operations, to name but a few. In a typical application, a single autonomous vehicle is managed by a crew using a ground station provided by the vehicle manufacturer. To execute more challenging missions, however, requires the use of multiple vehicles working together to achieve a common objective. Representative examples of cooperative mission scenarios are sequential auto-landing and coordinated ground target suppression for multiple UAVs. The first refers to the situation where a fleet of UAVs must break up and arrive at the assigned glideslope point, separated by pre-specified safe-guarding time-intervals. For the case of ground target suppression, a formation of UAVs must again break up and execute a coordinated maneuver to arrive at a predefined position over the target at the same time. In both cases, no absolute temporal constraints are given *a priori* - a critical point that needs to be emphasized. Furthermore, the vehicles must execute maneuvers in close proximity to each other. Thus the key requirement is that all maneuvers must be collision-free. As pointed

*Research is supported by USSOCOM, ONR under Contract N00014-05-1-0828, AFOSR under Contract No. FA9550-05-1-0157, ARO under Contract No. W911NF-06-1-0330, and EC under Contract 035223-GREX / CECIST.

†I. Kaminer, O. Yakimenko, V. Dobrokhodov are with Naval Postgraduate School, Monterey, CA 93943, e-mail: {kaminer, oayakime, vldobr}@nps.edu, A. Pascoal is with the Institute for Systems and Robotics (ISR) & Electrical Engineering and Computers, Instituto Superior Técnico (IST), Lisbon, Portugal, e-mail: antonio@isr.ist.utl.pt, N. Hovakimyan, C. Cao, A. Young, V. Patel are with Aerospace & Ocean Engineering, Virginia Polytechnic Institute & State University, Blacksburg, VA 24061, e-mail: {nhovakim, chengyu, ayoung83, vvp2069}@vt.edu.

out in Refs.,[29,31] the problem at hand poses new challenges to system designers. Among these, the following are worth stressing:

i) except for some cases of close formation flying like in Ref.,[26] the motion of one vehicle does not directly affect the motion of the other vehicles, that is, the vehicles are dynamically decoupled; the only coupling arises naturally out of the specification of the tasks that they are required to accomplish together.

ii) the flow of information among vehicles may be severely restricted, either for security reasons or because of tight bandwidth limitations. As a consequence, no vehicle will be able to communicate with the entire formation and the inter-vehicle communication network may change over time. It is therefore imperative to develop coordinated motion control strategies that can yield robust performance in the presence of communication failures and switching communication topologies. New paradigms are required to address this fundamental problem, departing from classical centralized control methodologies that deal with systems where a single (local) feedback controller possesses all the information needed to meet adequate stability and performance criteria. In fact, in many applications – including the ones described above – it is impractical for a central unit to have access to the state of the complete vehicle fleet. This makes it impossible to tackle the control problems at hand in the framework of centralized control theory. There is therefore a need for decentralized control architectures whereby a set of networked local controllers, having access to partial information only, perform together to meet a common goal. An example is to make identical subsets of the states of all systems in a network converge to common values (the agreement problem).

Motivated by these and similar problems, there has been over the past few years a flurry of activity in the area of multi-agent system networks with application to engineering and science problems. The range of topics addressed include parallel computing,[62] synchronization of oscillators,[53] study of collective behavior and flocking,[28] multi-system consensus mechanisms,[34] multi-vehicle system formations,[17] coordinated motion control,[23] asynchronous protocols,[18] dynamic graphs,[39] stochastic graphs,[39,56,57] and graph-related theory.[13,31] Especially relevant are the applications of the theory developed in the area of multi-vehicle formation control: spacecraft formation flying,[38] unmanned aerial vehicle (UAV) control,[55,58] coordinated control of land robots,[23] and control of multiple autonomous underwater vehicles (AUVs).[20,46,36]

In a typical theoretical setup, a cooperative control problem is reduced to an agreement or consensus problem whereby the topology of the inter-agents communication network is embodied in a communication graph. It has been shown (see for example Refs.[28,45,59]) that solutions to these problems result in flocking or swarming behaviors of the autonomous agents involved. However, stability and performance of these formations depend strongly on the nature of the underlying communication topology. Therefore, a major focus of current research is to analyze the impact of various communication models on stability and performance of the formations of autonomous agents. The studies in Ref.[19] address the situations where the communication topologies are fixed and bidirectional. Ref.[34] focuses on the more complicated case of fixed, unidirectional topologies. Time-varying network topologies in a deterministic setting are addressed in Refs.,[28,34,41] while stochastic models are used in Refs.[39,56,57] In Ref.,[39] state-dependent graphs are used to model the distance between agents or the signal strength in each link in the formation.

It is important to point out in the literature on cooperative control that the agents are usually modelled as identical single integrators,[28,41] nonholonomic integrators,[34,51,53] identical linear systems,[19] or special classes of linear systems.[32] Nonholonomic integrators are typically used to model dynamic systems such as AUVs,[53] robots,[34,35] and UAVs.[37,51,63] These simplified models may not be adequate to describe the dynamics of UAVs and AUVs as they undergo the maneuvers required to execute the complex missions of the type described above.

This paper presents a general framework for the problem of coordinated control of multiple autonomous agents that must operate under strict spatial and temporal constraints, while ensuring collision-free maneuvers. The proposed framework borrows from multiple disciplines and integrates algorithms for path generation, path following, time-critical coordination, and $\mathcal{L}_1$ adaptive control theory for fast and robust adaptation. Together, these techniques yield control laws that meet strict performance requirements in the presence of modeling uncertainties, environmental disturbances, and network failures. The methodology proposed in the paper is exemplified for the case of UAVs and unfolds in three basic steps.

First, given a multiple vehicle task, a set of feasible trajectories is generated for all UAVs using a direct method of calculus of variations that takes explicitly into account the initial and final boundary conditions, a general performance criterion to be optimized, the simplified UAV dynamics, and safety rules for collision

avoidance. This is done by resorting to an extension of the work reported in Refs.[60,64] on the generation of feasible aircraft trajectories for multiple UAVs. This step yields - for each vehicle - a spatial path to be followed. The key idea involved is to decouple space and time in the problem formulation. This reduces drastically the number of optimization parameters, making it easy to implement the optimization algorithms in real-time and guaranteeing that the computational complexity increases *only linearly* with the number of vehicles.

The second step consists of making each vehicle follow its assigned path while tracking a desired speed profile. Path following control design is first done at a kinematic level, leading to an outer-loop controller that generates pitch and yaw rate commands to an inner-loop controller. The latter relies on off-the-shelf autopilots for angular rate command tracking, augmented with an $\mathcal{L}_1$ adaptive output feedback control law that guarantees stability and performance of the complete system for each vehicle in the presence of modelling uncertainties and environmental disturbances. This methodology departs from standard backstepping techniques in that the final path following control law makes explicit use of existing UAV autopilots and yields "separation" of inner and outer control loop systems. The key factor that guarantees appropriate behaviour of the two subsystems put together is the introduction of an $\mathcal{L}_1$ adaptive control law that exploits the circle of ideas exposed in Ref.[6] The benefit of the $\mathcal{L}_1$ adaptive controller is its ability of fast and robust adaptation, as proven in Refs.[7,8,9,10,11,12] It has analytically computable performance bounds for a system's input and output signals in addition to its guaranteed time-delay margin.[9,10] The $\mathcal{L}_1$ adaptive controller has been augmented to existing controllers in several aircraft applications (see Refs.[2,5] for example) and has been found to exhibit excellent system performance. Since a typical autopilot is designed to provide waypoint control, the proposed framework significantly expands the span of their applications.

Note that path following implies tracking a given spatial path without regard to any temporal constraints using any feasible speed profile. Thus, the proposed path following algorithm is naturally compatible with path (rather than time) dependent trajectories generated in the first step. Notice also that using the space/time decomposition makes the speed profile of each vehicle an extra degree of freedom to be exploited in the time-coordination step.

Finally, in the third step the speed profile of each vehicle is adjusted about the nominal speed profile derived in the first step to enforce the temporal constraints that must be met in real-time in order to coordinate the entire fleet of AUVs. This step relies on the underlying communication network as a means of information exchange between the vehicles.

The methodology proposed relies on the decoupling of spatial and temporal assignments during the path generation, path following and coordination phases, respectively. From the above, it also follows that the solution advanced builds on three key ingredients: i) the use of direct methods of calculus of variations for real-time trajectory generation, ii) a path following strategy for the spatial assignment, and iii) a coordination or synchronization algorithm for multi-vehicle temporal assignment so as to achieve coordination. The last two techniques are well rooted in previous results reported in Ref.[24] on coordinated path following (CPF) control of multiple wheeled robots in the presence of bidirectional communication constrains. See also Ref.[54] for related work in the area of marine vehicles and Ref.[24] for the extension of the circle of ideas exploited in Ref.[23] to a very general class of vehicles and communication networks with intermittent failures, time-varying topologies, and delays. In Refs.,[23,24] the CPF problem is naturally split into two. At the lower (or inner-loop) level, the path-following problem is solved for individual vehicles, each having access to local measurements only. Coordination is achieved by synchronizing the so-called coordination states at the higher (or outer loop) level. The coordination level is supported by the communication network over which information is exchanged. The types of links available and the constraints they impose are captured in the framework of graph theory,[25] which is the tool par excellence to study the impact of communication topologies on the performance that can be achieved with coordination. A similar approach is pursued in the current paper, where tools from Lyapunov-based stability analysis, graph theory, and $\mathcal{L}_1$ adaptation are brought together to yield results on the overall coordinated behavior of a fleet of UAVs executing a variety of time-coordinated missions.

The paper is organized as follows. Section II introduces specific algorithms for path generation and path following algorithms for UAVs in 3D space. At this stage, path following is done at the kinematic level (outer-loop control). Section III describes an $\mathcal{L}_1$ adaptive augmentation technique for path following that yields an inner-loop control structure and exploits the availability of off-the-shelf autopilots for pitch and

yaw rates. Section IV derives a strategy for time-coordinated control of multiple UAVs at the kinematic level that relies on the adjustment of the desired speed profile of each vehicle. This is extended in Section V to include the vehicle dynamics by resorting to another $\mathcal{L}_1$ adaptive augmentation loop that makes use of existing speed of the autopilots. Section VI includes the stability proof of combined path-following and time-coordinated control strategies of multiple UAVs with $\mathcal{L}_1$ adaptive augmentation. Section VII describes actual flight test results performed in Camp Roberts, CA, in February and May of 2007 and includes a description of the hardware used in the configuration. The paper ends with the conclusions in Section VIII.

II. Path Following in 3D Space

This section describes algorithms for UAV path generation and path following in 3D space. We recall that a path is simply a curve $p_c : \tau \to \mathbb{R}^3$ parametrized by τ in a closed subset of $\mathbb{R}_+$, that is, $p_c = p_c(\tau)$. If τ is identified with time t or is a function thereof then, with a slight abuse of notation, $p_c(t) = p_c(\tau(t))$ will be called a trajectory. Path following refers to the problem of making a vehicle converge to and following a path $p_c(\tau)$ with no assigned time schedule. However, the vehicle speed may be assigned as a function of parameter τ. Trajectory tracking is the problem of making the vehicle track a trajectory $p_c(t)$, that is, the vehicle must meet simultaneous constraints in space and time.

II.A. Feasible Path Generation

Real time path generation that explicitly accounts for dynamic constraints is a critical requirement for the autonomous vehicles of today. In this section, we describe a path generation algorithm that is suitable for real-time computation of feasible trajectories for multiple UAVs that are de-conflicted in space and that can be followed by resorting to the path following algorithm described later in the paper. The key ideas involved can be best explained with the help of an example. Consider a fleet of n UAVs that are tasked to start from different locations and arrive at the same final target simultaneously. The exact time of arrival is not specified, but it may be restricted to lie within certain bounds.

Suppose the objective is to execute this multi-vehicle mission while avoiding inter-vehicle collisions, meeting dynamical constraints (e.g. bounds on maximum accelerations), and minimizing a weighted combination of vehicle energy expenditures. At first inspection, a possible solution to this problem would be to solve a constrained optimization problem that would yield (if at all possible) feasible trajectories $p_{c_i}(t), t \in [t_o, t_f]; i = 1, 2, ..., n$ for the vehicles, with t_o and t_f denoting initial and final time, respectively. Trajectory tracking systems on-board the UAVs would then ensure precise tracking of the trajectories generated, thus meeting the mission objectives.

This seemingly straightforward solution suffers from a major drawback: it does not allow for any "deviations from the plan". Absolute timing becomes crucial because the strategy described does not lend itself to on-line modification in the event that one or more of the vehicles cannot execute trajectory tracking accurately (e.g. due to adverse winds or lack of sufficient propulsion power). For this reason, it is far more practical to adopt a different solution where absolute time is not crucial and enough room is given to each vehicle to adjust its motion along the path in response to the motions of the other vehicles. The goal is that of reaching a terminal formation pattern that will ensure simultaneous arrival times. Dispensing with absolute time is key to the solution proposed. In this set-up, the optimization process should be viewed as a method to produce paths $p_{c_i}(\tau_i)$ without explicit time constraints, but with timing laws for $\tau_i(t)$ that effectively dictate how the nominal speed of each vehicle should evolve along the path. Using this set-up, spatial and temporal constraints are essentially decoupled and captured in the descriptions of $p_{c_i}(\tau_i)$ and $\eta_i(\tau) = d\tau_i/dt$, respectively, as will be seen later. Furthermore, adopting polynomial approximations for $p_{c_i}(\tau_i)$ and $\eta_i(\tau) = d\tau_i/dt$ keeps the number of optimization parameters reduced and makes real-time computational requirements easy to achieve. Intuitively, by making the path of a generic vehicle a polynomial function of $\tau \in [0, \tau_f]$, the shape of the path in space can be changed by increasing or decreasing τ - a single optimization parameter. This, coupled with a polynomial approximation for $\eta(\tau) = d\tau/dt$ makes it easy to shape the speed and acceleration profile of the vehicle along the path so as to meet desired dynamical constraints. The paths thus generated are the "templates" used for path following, as explained in Section II.B later in the paper.

The above circle of ideas was first explored in Refs.[42,60,61,64] for a single aircraft. This paper extends these results to the case of multiple UAVs following earlier work by the authors reported in Ref.[30] As will be seen, the approach to path generation exploits a separation between spatial and temporal specifications. Let $p_c(\tau) = [x(\tau), y(\tau), z(\tau)]^\top$ denote a desired path to be followed by a single UAV, parameterized by $\tau = [0; \tau_f]$. For computational efficiency, assume each coordinate $x(\tau), y(\tau), z(\tau)$ is represented by an algebraic polynomial of degree N of the form

$$x_i(\tau) \quad = \quad \sum_{k=0}^{N} a_{ik}\tau^k, \qquad i = 1, 2, 3, \tag{1}$$

where we set $x_1 = x, x_2 = y, x_3 = z$ for notational convenience. The degree N of polynomials $x_i(\tau)$ is determined by the number of boundary conditions that must be satisfied. Notice that these conditions (that involve spatial derivatives) are computed with respect to the parameter τ. There is an obvious need to relate them to actual temporal derivatives, but this issue will only be addressed later. For the time being, let d_0 and d_f be the highest-order of the spatial derivatives of $x_i(\tau)$ that must meet specified boundary constraints at the initial and final points of the path, respectively. Then, the minimum degree N^* of each polynomial in (1) is $N^* = d_0 + d_f + 1$. For example, if the desired path includes constraints on initial and final positions, velocities, and accelerations (second-order derivatives), then the degree of each polynomial is $N^* = 2 + 2 + 1 = 5$. Explicit formulae for computing boundary conditions $p_c'(0), p_c''(0)$ and $p_c'(\tau_f), p_c''(\tau_f)$ are given later in this section. Additional degrees of freedom may be included by making $N > N^*$. As an illustrative example, Table 1 shows how to compute the polynomial coefficients in (1) for polynomial trajectories of 5^{th} and 6^{th} degree. For 6^{th} degree polynomial trajectories, an additional constraint on the fictitious initial jerk is included, which increases the order of the resulting polynomial and affords extra (design) parameters $x_i'''(0); i = 1, 2, 3$. Figure 1 shows examples of admissible 5^{th} and 6^{th} order polynomial paths when only τ_f or τ_f and $x_i'''(0); i = 1, 2, 3$, viewed as optimization parameters, vary. Figure 1 (right) shows how an increase in the number of optimization parameters leads to a larger class of admissible paths (in this particular case, parameters corresponding to initial jerk are added as free variables).

It is now important to clarify how temporal constraints may be included in the feasible path computation process. A trivial solution would be to make $\tau = t$. In this case, solving the polynomial fitting problem that is at the root of Fig. 1 yields the speed profiles of Fig. 2. Little control exists over the resulting speeds even with fifth and sixth order polynomials, because once $x_1(t), x_2(t), x_3(t)$ have been computed to satisfy the boundary constraints imposed, speed v is inevitably given by

$$v(t) \quad = \quad \sqrt{\dot{x}_1^2(t) + \dot{x}_2^2(t) + \dot{x}_3^2(t)}. \tag{2}$$

We therefore turn our attention to a different procedure that will afford us the possibility of meeting strict boundary conditions and constraints without increasing the complexity of the path generation process. To this effect, let $v_{\min}, v_{\max}$ and $a_{\max}$ denote predefined bounds on the vehicle's speed and acceleration, respectively. Let $\eta(\tau) = d\tau/dt$, yet to be determined, dictate how parameter τ evolves in time. A path $p_c(\tau)$ (with an underlying assignment $\eta(\tau)$) is said to constitute a *feasible* path if the resulting trajectory can be tracked by an UAV without exceeding prespecified bounds on its velocity and total acceleration along that trajectory. With an obvious use of notation, we will later refer to a spatial path only, without the associated $\eta(\tau)$, as a feasible path.

From (2), and for a given choice of $\eta(\tau)$, the temporal speed $v_p(\tau(t))$ and acceleration $a_p(\tau(t))$ of the vehicle along the path (abbv. $v_p(\tau)$ and $v_p(\tau)$, respectively) are given by

$$\begin{aligned} v_p(\tau) \; &= \; \eta(\tau)\sqrt{x_1'^2(\tau) + x_2'^2(\tau) + x_3'^2(\tau)} \; = \; \eta(\tau)||p_c'(\tau)||, \\ a_p(\tau) \; &= \; ||p_c''(\tau)\eta^2(\tau) + p_c'(\tau)\eta'(\tau)\eta(\tau)||. \end{aligned} \tag{3}$$

Table 1. Examples of computation of the coefficients of 5^{th} and 6^{th} order polynomial paths.

5^{th} order	
Boundary conditions	$x_i(0), x_i'(0), x_i''(0), x_i(\tau_f), x_i'(\tau_f), x_i''(\tau_f)$
d_0/d_f	2/2
N^*/N	5/5
Linear algebraic matrix equation to solve for the coefficients a_{ik}	$\begin{bmatrix} 1 & 0 & 0 & 0 & 0 & 0 \\ 0 & 1 & 0 & 0 & 0 & 0 \\ 0 & 0 & 2 & 0 & 0 & 0 \\ 1 & \tau_f & \tau_f^2 & \tau_f^3 & \tau_f^4 & \tau_f^5 \\ 0 & 1 & 2\tau_f & 3\tau_f^2 & 4\tau_f^3 & 5\tau_f^4 \\ 0 & 0 & 2 & 6\tau_f & 12\tau_f^2 & 20\tau_f^3 \end{bmatrix} \begin{bmatrix} a_{i0} \\ a_{i1} \\ a_{i2} \\ a_{i3} \\ a_{i4} \\ a_{i5} \end{bmatrix} = \begin{bmatrix} x_i(0) \\ x_i'(0) \\ x_i''(0) \\ x_i(\tau_f) \\ x_i'(\tau_f) \\ x_i''(\tau_f) \end{bmatrix}$

6^{th} order	
Boundary conditions	$x_i(0), x_i'(0), x_i''(0), x_i'''(0), x_i(\tau_f), x_i'(\tau_f), x_i''(\tau_f)$
d_0/d_f	3/2
N^*/N	5/6
Linear algebraic matrix equation to solve for the coefficients a_{ik}	$\begin{bmatrix} 1 & 0 & 0 & 0 & 0 & 0 & 0 \\ 0 & 1 & 0 & 0 & 0 & 0 & 0 \\ 0 & 0 & 2 & 0 & 0 & 0 & 0 \\ 0 & 0 & 0 & 6 & 0 & 0 & 0 \\ 1 & \tau_f & \tau_f^2 & \tau_f^3 & \tau_f^4 & \tau_f^5 & \tau_f^6 \\ 0 & 1 & 2\tau_f & 3\tau_f^2 & 4\tau_f^3 & 5\tau_f^4 & 6\tau_f^5 \\ 0 & 0 & 2 & 6\tau_f & 12\tau_f^2 & 20\tau_f^3 & 30\tau_f^4 \end{bmatrix} \begin{bmatrix} a_{i0} \\ a_{i1} \\ a_{i2} \\ a_{i3} \\ a_{i4} \\ a_{i5} \\ a_{i6} \end{bmatrix} = \begin{bmatrix} x_i(0) \\ x_i'(0) \\ x_i''(0) \\ x_i'''(0) \\ x_i(\tau_f) \\ x_i'(\tau_f) \\ x_i''(\tau_f) \end{bmatrix}$

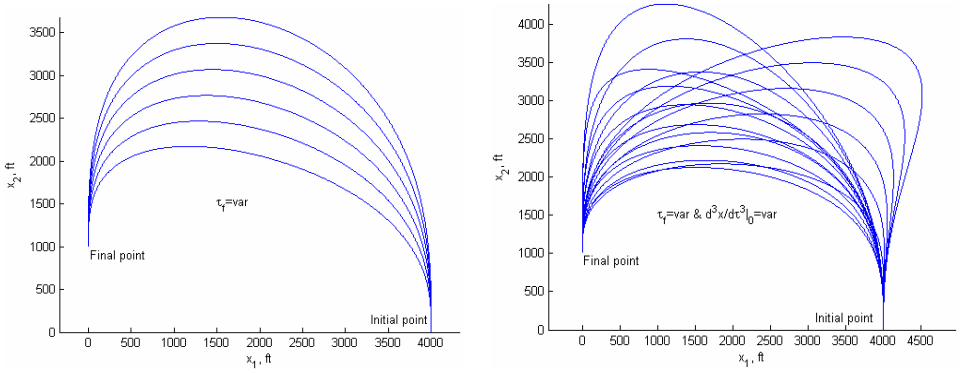

Figure 1. Admissible trajectories for 5^{th} and 6^{th} order polynomials.

At this point, a choice for $\eta(\tau)$ must be made. A particular choice is simply $\eta(\tau) = \eta(0) + \frac{\tau}{\tau_f}(\eta(f) - \eta(0))$ with $\eta(0) = v_p(0)$ and $\eta(\tau_f) = v_p(t_f)$, where t_f is the terminal time yet to be determined. This polynomial is of degree sufficiently high to satisfy boundary conditions on speed and acceleration. This follows from the fact that the boundary conditions $p_c'(0), p_c''(0), p_c'(\tau_f), p_c''(\tau_f)$ can be easily obtained from given $\dot{p}_c(0), \ddot{p}_c(0)$,

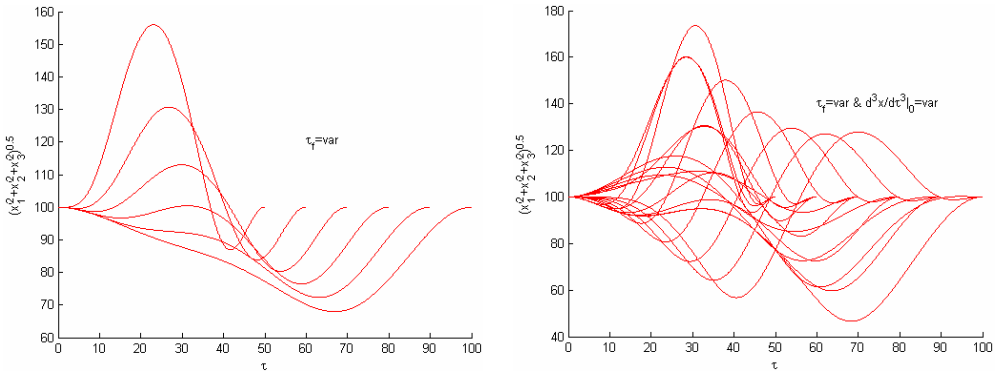

Figure 2. Speed profile corresponding to the paths shown in Figure 1 when $\tau = t$. Left: varying τ_f. Right: varying τ_f and the initial jerk.

.

$\dot{p}_c(t_f), \ddot{p}_c(t_f)$ using the definition of $\eta(\tau)$. In fact, since $\dot{p}_c(t) = p_c'(\tau)\eta(\tau)$, it is easy to see that

$$\begin{aligned} p_c'(0) &= \frac{\dot{p}_c(0)}{\eta(0)}, \\ p_c'(\tau_f) &= \frac{\dot{p}_c(t_f)}{\eta(\tau_f)}, \\ p_c''(0) &= \frac{\ddot{p}_c(0) - p_c'(0)\eta'(0)\eta(0)}{\eta^2(0)}, \\ p_c''(\tau_f) &= \frac{\ddot{p}_c(t_f) - p_c'(t_f)\eta'(\tau_f)\eta(\tau_f)}{\eta^2(\tau_f)}, \end{aligned}$$

where $\eta'(0) = \eta'(\tau_f) = \frac{\eta(\tau_f)-\eta(o)}{\tau_f}$. Furthermore, the choice of boundary conditions on $\eta(\tau)$ guarantees that $||p_c'(0)|| = ||p_c'(t_f)|| = 1$.

It now follows from (3) that a path $p_c(\tau)$ is feasible if all boundary conditions are met, together with the additional speed and acceleration constraints

$$v_{\min} \leq \eta(\tau)\ ||p_c'(\tau)|| \leq v_{\max}, \qquad ||p_c''(\tau)\eta^2(\tau) + p_c'(\tau)\eta'(\tau)\eta(\tau)|| \leq a_{\max},\ \forall \tau \in [0, \tau_f]. \tag{4}$$

A feasible trajectory can be obtained by solving, for example, the optimization problem

$$F1 : \min_{\Xi} J \quad \textit{subject to } (4)$$

and to the boundary conditions at initial and final points, where Ξ is the vector of optimization parameters that includes either τ_f or τ_f and $x_i'''(0)$ for $i = 1, 2, 3$. The latter definition of Ξ corresponds to the case where the degree of the polynomial path is selected to be 6 (see Table 1). The cost function J may be defined to be the total fuel consumption of the UAV given by

$$J = \int_0^{t_f} c_f c_D \rho v_c^3(t) dt = \int_0^{\tau_f} c_f c_D \rho \eta^3(\tau)\ ||p_c'(\tau)||^3\ d\tau,$$

where ρ is dynamic pressure, c_f is the specific fuel consumption constant, and c_D is the total drag coefficient of the UAV. Other choices of J can be made to address time optimal or minimum length paths.

In this paper, the above methodology is extended to the case of multiple UAVs. In particular, we address the problem of time-coordinated control where all UAV's must arrive at their respective final destinations at the same time. The dimension of the corresponding optimization problem increases and the time coordination requirement introduces additional constraints on parameters $\tau_{fi}; i = 1, 2, .., n$. Without loss of generality, we

compute the total time of flight t_{f1} for UAV 1. A similar procedure can be used to compute the times of flight $t_{fi}; i = 2, .., n$. Using the definition of $\eta_i(\tau)$,

$$t_{f1} = \int_0^{\tau_{f1}} \frac{d\tau_1}{\eta_1(\tau_1)}.$$

It follows immediately that the minimum time of flight $t_{f1_{\min}}$ of UAV 1 is given by

$$t_{f1_{\min}} = \int_0^{\tau_{f1}} \frac{||p_1'(\tau_1)||\ d\tau_1}{v_{\max_1}}.$$

Similarly, its maximum time of flight is

$$t_{f1_{\max}} = \int_0^{\tau_{f1}} \frac{||p_1'(\tau_1)||\ d\tau_1}{v_{\min_1}}.$$

Hence, UAV 1 will arrive at the target in the interval $T_1 = [t_{f1_{\min}}, t_{f1_{\max}}]$. Let $T_i = [t_{fi_{\min}}, t_{fi_{\max}}]$ denote the time interval for the arrival of UAV i at its assigned target. Clearly, the time coordinated problem has a solution *if and only if* $T_i \bigcap T_j \neq \emptyset\ \forall i, j = 1, \ldots, n, i \neq j$. This is guaranteed if $\min_i t_{fi_{\max}} \geq \max_i t_{fi_{\min}}$ for $i = 1, \ldots, n$. Thus, for the case of multiple UAVs additional constraints must be imposed on $\tau_{fi}; i = 1, .., n$. Feasible, spatially deconflicted trajectories for all vehicles can be obtained by solving an optimization problem of the form

$$F2 : \begin{cases} \min\limits_{\Xi_i, i=1,\ldots,n} \sum\limits_{i=1}^{n} w_i J_i \textit{ subject to boundary conditions and (4) for any } i \in [1, n] \textit{ and} \\ \min\limits_{j,k=1,\ldots,n, j\neq k} ||p_{c_j}(\tau_j) - p_{c_k}(\tau_k)||^2 \geq E^2 \textit{ for any } \tau_j, \tau_k \in [0, \tau_{fj}] \times [0, \tau_{fk}], \\ \min\limits_i t_{fi_{\max}} \geq \max\limits_i t_{fi_{\min}}, \textit{for } i = 1, \ldots, n, \end{cases} \tag{5}$$

where J_i represents total fuel consumption of UAV i and the weights $w_i > 0$ penalize the energy consumptions of all UAVs $i \in [1, n]$. Note that in $F2$ an additional constraint $\min_{j,k=1,\ldots,n, j\neq k} ||p_{c_j}(\tau_j) - p_{c_k}(\tau_k)||^2 \geq E^2$ for any $\tau_j, \tau_k \in [0, \tau_{fj}] \times [0, \tau_{fk}]$ was added to guarantee spatially deconflicted trajectories separated by a minimum distance E. In addition, we emphasize that the dimension of the optimization problem $F2$ increases linearly with the number of UAVs.

The optimization problems $F1, F2$ can be effectively solved in real-time by adding a penalty function G as discussed in Ref.[64] and by using any zero-order optimization technique. As an example, Fig. 3 illustrates the flexibility afforded by the reference polynomials to compute a coordinated target reconnaissance mission by three UAVs. In this case, $\Xi = [\tau_{f1}\ \ \tau_{f2}\ \ \tau_{f3}]$. The final value of the optimization parameter vector $\Xi_{final} = [5512.8\ \ 7771.9\ \ 10217.0]$ resulted in spatially deconflicted paths where the minimum distance between any two paths did not fall below 349 m (the minimum required distance was 100 m). Furthermore, the nominal speed profiles shown in Fig. 4 stayed within the predefined limits of $[v_{\min}\ \ v_{\max}] = [15m/sec\ \ 25m/sec]$. The selected speed limits were below the physical capabilities of the UAVs used in the flight tests. This was done to ensure that each path can be tracked in the presence of winds. The maximum acceleration corresponding to each path did not exceed $0.6m/sec^2$, well below the limit of $0.5g$. It is important to point out that these profiles simply confirm that each path is indeed feasible. They will not be used directly by the controllers discussed in the following sections. In fact, coordinated speed references that depend on the true speed of the leader along its path will be generated online to guarantee time coordination of the UAVs. Finally, the intervals τ_i for $i = 1, 2, 3$ were computed to be $[203.47\ \ 508.66], [281.39\ \ 703.48]$, and $[408.66\ \ 1021.70]$ respectively. Their intersection $[408.66\ \ 508.66]$ is 100 seconds long - sufficient duration to guarantee that UAVs 2 and 3 can arrive at their respective destinations at the same time as UAV 1. This situation is illustrated in Figure 5.

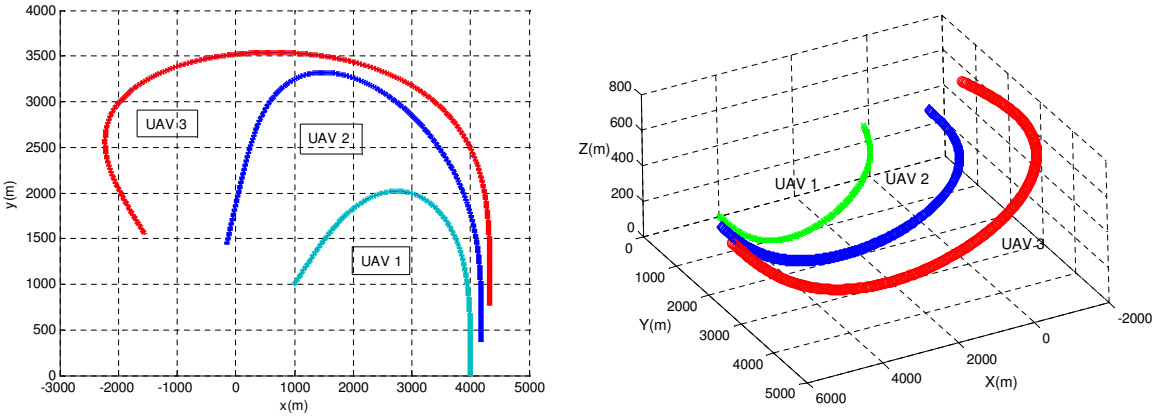

Figure 3. Example of spatially deconflicted trajectories. Top view, moving from right to left (left), 3D view, moving from left to right (right).

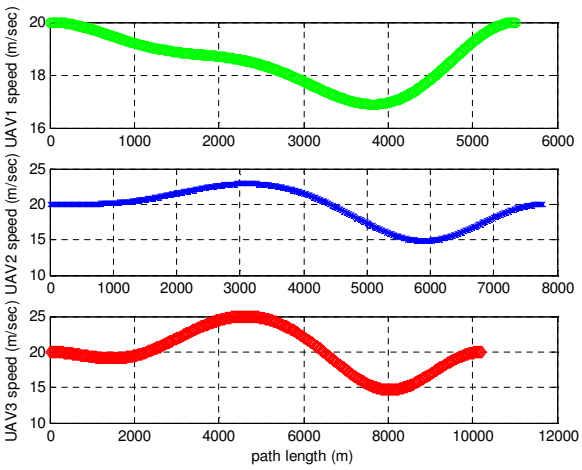

Figure 4. Feasible speed profiles for each UAV.

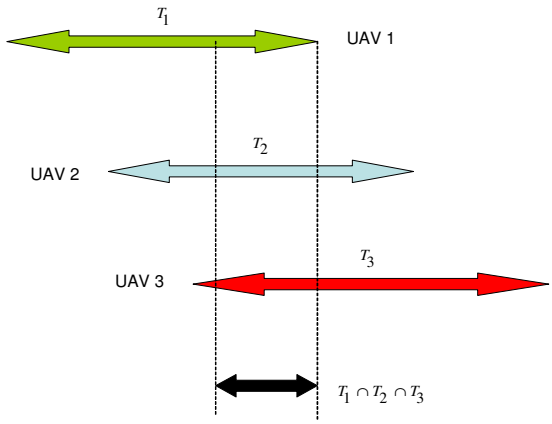

Figure 5. Intersection of time intervals T_i for each UAV.

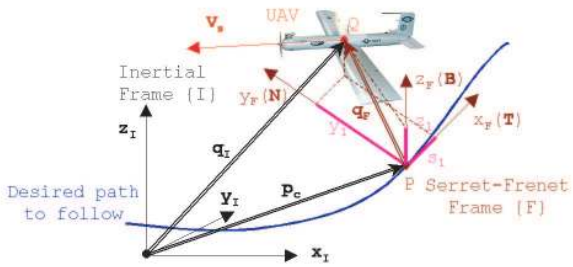

Figure 6. Problem Geometry

II.B. Path Following of the Polynomial Trajectories using UAV Kinematics

In order for each vehicle to follow the spatial path generated by the methodology introduced above, a path following algorithm that extends the one in Ref.[52] to a 3D setting is introduced with a further modification aimed at meeting time-critical and inter-vehicle constraints. At this level, only the simplified kinematic equations of the vehicle will be addressed by taking pitch rate and yaw rate as virtual outer-loop control inputs. The dynamics are dealt with in Section III by introducing an inner-loop control law via the novel $\mathcal{L}_1$ adaptive output feedback controller. The required notation is introduced with reference to Fig. 6. Let F be a Serret-Frenet frame attached to a generic point on the path, and let W be the wind frame attached to the UAV center of mass Q (a frame that has its x-axis aligned with the UAV's velocity vector). Further let ω_{FI}^{F} denote the angular velocity of F with respect to the inertial frame I, resolved in F. Let $p_c(\tau)$ be the path to be followed by a UAV and P be an arbitrary point on the path that plays the role of the center of mass of a "virtual" aircraft to be followed. This is a different approach as compared to the set-up for path following originally proposed in Ref.,[40] where P was simply defined as the point on the path that is closest to the vehicle. Since this point may not be uniquely defined, the strategy in Ref.[40] led to more conservative estimates for the region of attraction about the path to be followed which we wish to relax. Endowing P with an extra degree of freedom is the key to the algorithm presented in Ref.,[52] which is extended in this paper to the 3D case. Notice that Q can be resolved in I as $q_I = [x_I \; y_I \; z_I]^\top$ or in F as $q_F = [x_F \; y_F \; z_F]^\top$. With the above notation, the simplified UAV kinematic equations can be written as

$$\begin{cases} \dot{x}_I = v\cos\gamma\cos\psi \\ \dot{y}_I = -v\cos\gamma\sin\psi \\ \dot{z}_I = v\sin\gamma \\ \begin{bmatrix} \dot{\gamma} \\ \dot{\psi} \end{bmatrix} = \begin{bmatrix} 1 & 0 \\ 0 & \cos^{-1}\gamma \end{bmatrix} \begin{bmatrix} q \\ r \end{bmatrix}, \end{cases} \tag{6}$$

where v is the magnitude of the UAV's velocity vector, γ is the flight path angle, ψ is the heading angle, and q, r are the y-axis and z-axis components, respectively of the vehicle's rotational velocity resolved in wind frame W. For the purpose of this paper, q and r will be referred to as pitch rate and yaw rate, respectively in the wind frame W.

Following standard nomenclature,[29,15] let l denote the path length along the desired path p_c. Note, that for infinitesimal perturbations along the path dp_c and dl, we obtain that $||dp_c|| = ||dl||$. Therefore, $||dp_c/dl|| = 1$ and

$$\frac{dp_c}{d\tau} = \frac{dp_c}{dl}\frac{dl}{d\tau} \Rightarrow \left|\frac{dl}{d\tau}\right| = \left\|\frac{dp_c}{d\tau}\right\| = \|p_c'(\tau)\|.$$

Thus $\left|\frac{dl}{d\tau}\right| = \|p_c'(\tau)\|$ defines a differential relationship between l and τ. Next we derive the unit vectors T, N, B that define the Frenet frame F attached to the path $p_c(l)$ at a point defined by l. Let

$$\begin{aligned} T(l) &= \frac{dp_c(l)}{dl} \Big/ \left\| \frac{dp_c(l)}{dl} \right\|, \\ N(l) &= \frac{dT(l)}{dl} \Big/ \left\| \frac{dT(l)}{dl} \right\|, \\ \text{and } B(l) &= T(l) \times N(l). \end{aligned}$$

Then these vectors respectively define the tangent, normal, and binormal to the path at the point determined by l. The vectors T, N, B are orthonormal and represent the basis vectors of F and can be used to construct the rotation matrix $R_F^I = [T\ N\ B]$ from F to I. It is well known that

$$\dot{R}_F^I = R_F^I S(\omega_{FI}^F) \tag{7}$$

and that $\omega_{FI}^F = [\zeta \dot{l} \quad 0 \quad \kappa \dot{l}]^\top$, where S is a skew-symmetric operator induced by the elements of ω_{FI}^F, $\kappa(l) = \left\| \frac{dT(l)}{dl} \right\|$ is the curvature of $p_c(l)$ and $\zeta(l) = \left\| \frac{dB(l)}{dl} \right\|$ is its torsion. Using equation (7) and Fig. 6 we obtain

$$q_I = p_c(l) + R_F^I q_F,$$

and therefore

$$\dot{q}_I = R_F^I \begin{bmatrix} \dot{l} \\ 0 \\ 0 \end{bmatrix} + R_F^I \begin{bmatrix} \dot{x}_F \\ \dot{y}_F \\ \dot{z}_F \end{bmatrix} + R_F^I \left(w_{FI}^F \times \begin{bmatrix} \dot{x}_F \\ \dot{y}_F \\ \dot{z}_F \end{bmatrix} \right). \tag{8}$$

Using (8) and the fact that

$$R_I^F \begin{bmatrix} \dot{x}_I \\ \dot{y}_I \\ \dot{z}_I \end{bmatrix} = R_W^F R_I^W \begin{bmatrix} \dot{x}_I \\ \dot{y}_I \\ \dot{z}_I \end{bmatrix} = R_W^F \begin{bmatrix} v \\ 0 \\ 0 \end{bmatrix},$$

where R_W^F and R_I^W are the rotation matrices from W to F and I to W respectively, we obtain

$$R_I^F \begin{bmatrix} \dot{x}_I \\ \dot{y}_I \\ \dot{z}_I \end{bmatrix} = \begin{bmatrix} \dot{l}(1 - \kappa y_F) + \dot{x}_F \\ \dot{y}_F + \dot{l}(\kappa x_F - \zeta z_F) \\ \dot{z}_1 + \zeta \dot{l} y_F \end{bmatrix}$$

and

$$\begin{bmatrix} \dot{x}_F \\ \dot{y}_F \\ \dot{z}_F \end{bmatrix} = \begin{bmatrix} -\dot{l}(1 - \kappa y_F) \\ -\dot{l}(\kappa x_F - \zeta z_F) \\ -\zeta \dot{l} y_F \end{bmatrix} + R_W^F \begin{bmatrix} v \\ 0 \\ 0 \end{bmatrix}. \tag{9}$$

Let λ_e denote the Euler angles ϕ_e, θ_e, ψ_e that parameterize locally the rotation matrix from F to W. Then $\dot{\lambda}_e = Q^{-1}(\lambda_e)\ \omega_{WF}^W$, where

$$Q^{-1}(\lambda_e) = \begin{bmatrix} 1 & \sin\phi_e \tan\theta_e & \cos\phi_e \tan\theta_e \\ 0 & \cos\phi_e & -\sin\phi_e \\ 0 & \frac{\sin\phi_e}{\cos\theta_e} & \frac{\cos\phi_e}{\cos\theta_e} \end{bmatrix}, \tag{10}$$

is nonsingular for $\theta_e \neq \pm\frac{\pi}{2}$, and ω_{WF}^W denotes the angular velocity of W with respect to F resolved in W. Note that $\omega_{WF}^W = \omega_{WI}^W - \omega_{FI}^W$ and $\omega_{FI}^W = R_F^W\ \omega_{FI}^F$. Thus,

$$\dot{\lambda}_e = Q^{-1}(\lambda_e) \left(\omega_{WI}^W - R_F^W(\lambda_e) \omega_{FI}^F \right)$$

and

$$\begin{bmatrix} \dot{\theta}_e \\ \dot{\psi}_e \end{bmatrix} = \underbrace{\begin{bmatrix} \sin\psi_e \zeta \dot{l} \\ -\dot{l}(\zeta \tan\theta_e \cos\psi_e + \kappa) \end{bmatrix}}_{\equiv D} + \underbrace{\begin{bmatrix} \cos\phi_e & -\sin\phi_e \\ \frac{\sin\phi_e}{\cos\theta_e} & \frac{\cos\phi_e}{\cos\theta_e} \end{bmatrix}}_{\equiv G} \begin{bmatrix} q \\ r \end{bmatrix}, \tag{11}$$

where D and G are defined for all $\theta_e \neq \pm\frac{\pi}{2}$. Let

$$\begin{bmatrix} q \\ r \end{bmatrix} = G^{-1}\left(\begin{bmatrix} u_\theta \\ u_\psi \end{bmatrix} - D \right), \tag{12}$$

where u_θ and u_ψ are control inputs that have yet to be defined. Then, combining equations (9) and (12) yields the equations for the (path following) kinematic error dynamics:

$$\begin{aligned} & \dot{x}_F(t) = -\dot{l}(t)(1-\kappa(l(t))y_F(t)) + v(t)\cos(\theta_e(t))\cos(\psi_e(t)) \\ & \dot{y}_F(t) = -\dot{l}(t)(\kappa(l(t))x_F(t) - \zeta(l(t))z_F(t)) + v(t)\cos(\theta_e(t))\sin(\psi_e(t)) \\ & \dot{z}_F(t) = -\zeta(l(t))\dot{l}(t)y_F(t) - v(t)\sin(\theta_e(t)) \\ \mathcal{G}_e: \ & \dot{\theta}_e(t) = u_\theta(t) \\ & \dot{\psi}_e(t) = u_\psi(t) \\ & \dot{l}(t) = K_1 x_F(t) + v(t)\cos(\theta_e(t))\cos(\psi_e(t)) \\ & y(t) = [u_\theta(t)\ u_\psi(t)]^\top, \end{aligned} \tag{13}$$

where $K_1 > 0$ is a constant and $y(t)$ is the vector of the input signals u_θ and u_ψ which have yet to be designed. We assume that the speed profile of the UAV along the path is bounded below by $v_{\min} > 0$:

$$v(t) \geq v_{\min}, \quad \forall\ t \geq 0. \tag{14}$$

Let

$$x(t) = [x_F(t)\ \ y_F(t)\ \ z_F(t)\ \ \theta_e(t) - \delta_\theta(t)\ \ \psi_e(t) - \delta_\psi(t)]^\top,$$

where

$$\begin{aligned} \delta_\theta(t) &= \sin^{-1}\left(\frac{z_F(t)}{|z_F(t)| + d_1}\right), \\ \delta_\psi(t) &= \sin^{-1}\left(\frac{y_F(t)}{|y_F(t)| + d_2}\right), \end{aligned} \tag{15}$$

where $d_1 > 0\,,\ d_2 > 0$ are positive constants. Note that any choice of d_1 and d_2 guarantees $|\delta_\theta(t)|, |\delta_\psi(t)| < \frac{\pi}{2}$. For simplicity, we choose $d_1 = d_2$. Furthermore, define positive c_1, c_2 and d such that:

$$\alpha \triangleq \sqrt{2c_2/c_1}\ d + \sin^{-1}\frac{\sqrt{2}\ d}{d_1 + \sqrt{2}\ d} < \frac{\pi}{2}\,. \tag{16}$$

Note, since $\sin^{-1}\left(\frac{\sqrt{2}d}{d_1+\sqrt{2}d}\right) < \pi/2$, there always exist c_1, c_2 and d that verify (16). Let $y_c(t) = [u_{\theta_c}(t)\ \ u_{\psi_c}(t)]^\top$, with

$$\begin{aligned} u_{\theta_c}(t) &= -K_2(\theta_e(t) - \delta_\theta(t)) + \frac{c_2}{c_1} z_F(t) v(t) \frac{\sin(\theta_e(t)) - \sin(\delta_\theta(t))}{\theta_e(t) - \delta_\theta(t)} + \dot{\delta}_\theta(t) \\ u_{\psi_c}(t) &= -K_3(\psi_e(t) - \delta_\psi(t)) - \frac{c_3}{c_1} y_F(t) v(t)\cos(\theta_e(t)) \frac{\sin(\psi_e(t)) + \sin(\delta_\psi(t))}{\psi_e(t) - \delta_\psi(t)} + \dot{\delta}_\psi(t) \end{aligned} \tag{17}$$

for some positive constants K_2 and K_3. It follows from[30] that $\mathcal{G}_e$ can be stabilized by the functions in (17) as stated in the following lemma.

Lemma 1 *For any $v(t)$ verifying (14), if c_1, c_2, d, d_1 are chosen to satisfy (16), the kinematic error equations in (13) with the controllers $u_\theta(t) = u_{\theta_c}(t)$, $u_\psi(t) = u_{\psi_c}(t)$ defined in (17), are exponentially stable with the domain of attraction*

$$\Omega = \left\{ x : V_c(x) \leq \frac{d^2}{2c_1} \right\}, \tag{18}$$

where

$$V_c(t) = x^\top(t) P x(t), \qquad P = \text{diag}\left(\frac{1}{2c_1} \; \frac{1}{2c_1} \; \frac{1}{2c_1} \; \frac{1}{2c_2} \; \frac{1}{2c_2} \right). \tag{19}$$

Proof. It follows from (13) and (17) that

$$\begin{aligned}
\dot{V}_c &= \frac{x_F}{c_1}(-\dot{l}(1-\kappa y_F) + v\cos(\theta_e)\cos(\psi_e)) + \frac{y_F}{c_1}(-\dot{l}(\kappa x_F - \zeta z_F) + v\cos(\theta_e)\sin(\psi_e)) + \frac{z_F}{c_1} \\
&\quad (-\zeta \dot{l} y_F - v\sin(\theta_e)) + \frac{\theta_e - \delta_\theta}{c_2}(u_{\theta_c}(t) - \dot{\delta}_\theta) + \frac{\psi_e - \delta_\psi}{c_2}(u_{\psi_c} - \dot{\delta}_\psi) \\
&= \frac{-x_F\dot{l} + v\cos(\theta_e)(x_F\cos(\psi_e) + y_F\sin(\psi_e))}{c_1} + \frac{-z_F v\sin(\theta_e)}{c_1} - \frac{K_2}{c_2}(\theta_e - \delta_\theta)^2 - \frac{K_3}{c_2}(\psi_e - \delta_\psi)^2 + \\
&\quad \frac{v z_F(\sin(\theta_e) - \sin(\delta_\theta))}{c_1} - \frac{y_F v\cos(\theta_e)(\sin(\psi_e) + \sin(\delta_\psi))}{c_1} \\
&= -\frac{K_1}{c_1}x_F^2 - \frac{K_2}{c_2}(\theta_e - \delta_\theta)^2 - \frac{K_3}{c_2}(\psi_e - \delta_\psi)^2 - \frac{v y_F\sin(\delta_\psi)\cos(\theta_e) + v z_F\sin(\delta_\theta)}{c_1}
\end{aligned} \tag{20}$$

Using (15), we have

$$\dot{V}_c = -\frac{K_1}{c_1}x_F^2 - \frac{K_2}{c_2}(\theta_e - \delta_\theta)^2 - \frac{K_3}{c_2}(\psi_e - \delta_\psi)^2 - \frac{v z_F^2}{c_1(|z_F| + d_1)} - \frac{v\cos(\theta_e) y_F^2}{c_1(|y_F| + d_2)} = -x^\top Q x, \tag{21}$$

where

$$Q = \text{diag}\left(\frac{K_1}{c_1} \; \frac{v\cos(\theta_e)}{c_1(|y_F| + d_2)} \; \frac{v}{c_1(|z_F| + d_1)} \; \frac{K_2}{c_2} \; \frac{K_3}{c_2} \right). \tag{22}$$

Note that over the compact set Ω, the following upper bounds hold:

$$\begin{aligned}
|x_F(t)| &\leq d \\
|y_F(t)| &\leq d \\
|z_F(t)| &\leq d \\
|\theta_e(t)| &\leq \sqrt{\frac{c_2 d^2}{c_1}} + \sup(\delta_\theta(t)) = \sqrt{\frac{c_2 d^2}{c_1}} + \sin^{-1}\left(\frac{d}{d_1 + d}\right) < \frac{\pi}{2} \\
|\psi_e(t)| &\leq \sqrt{\frac{c_2 d^2}{c_1}} + \sup(\delta_\psi(t)) = \sqrt{\frac{c_2 d^2}{c_1}} + \sin^{-1}\left(\frac{d}{d_2 + d}\right) < \frac{\pi}{2},
\end{aligned} \tag{23}$$

where we have used the relationship (16) and the fact that $d_1 = d_2$ and $c = \frac{d^2}{2c_1}$. It follows from (22) and (23) that $Q \geq Q_c$, where

$$Q_c = \text{diag}\left(\frac{K_1}{c_1} \; \frac{v_{\min}\cos\alpha}{c_1(d + d_2)} \; \frac{v_{\min}}{c_1(d + d_1)} \; \frac{K_2}{c_2} \; \frac{K_3}{c_2} \right). \tag{24}$$

Since $Q_c > 0$ and

$$\dot{V}_c(t) \leq -x^\top(t) Q_c x(t) \quad \forall\, t \geq 0, \tag{25}$$

then $x(t)$ is exponentially stable over the compact set Ω, which completes the proof. □

Remark 1 *Notice that the solution to the path following problem assumes only that $v(t)$ is bounded below but is otherwise undefined. This extra degree of freedom is due to the decoupling of space and time in the problem formulation, which allows for the use of $v(t)$ at a later stage for coordination in time.*

III. $\mathcal{L}_1$ Adaptive Output Feedback Augmentation for Path Following in the Presence of Autopilot

III.A. $\mathcal{L}_1$ Adaptive Output Feedback Controller

As discussed above decoupling of space and time in the problem formulation allows for path following and coordination to be solved independently. To achieve the objective of time-critical coordination of UAVs, we need to ensure that the velocity profile for each UAV along its corresponding path – yet to be determined in the coordination step – matches the *a priori* specified bounds defined in the path generation step. Thus, for every UAV one needs to define the rate inputs u_θ (pitch) and u_ψ (yaw) to the autopilot and the speed profile v (velocity) along the path. The first two control signals must achieve the path following objective, while the velocity command should be exploited for coordination in time. Since the commercial autopilots are designed only to track simple way-point commands, in this section we modify the pitch and yaw rates from (17) – by augmenting those with $\mathcal{L}_1$-adaptive loops – to ensure that the UAV can follow the path defined in the path generation step. Recall that the controller in (17) was derived from purely kinematic considerations. The $\mathcal{L}_1$ adaptive augmentation presented in this section allows to account for the UAV dynamics.

To this end, we consider the complete system of kinematic error equations defined as subsystem $\mathcal{G}_e$ along with subsystem $\mathcal{G}_p$, which models the closed-loop system of the UAV with the autopilot:

$$\mathcal{G}_e : \dot{x}(t) = f(x(t)) + g(x(t))y(t) \tag{26}$$
$$\mathcal{G}_p : y(s) = G_p(s)(u(s) + z(s)), \tag{27}$$

where $y(s)$ and $u(s)$ are the Laplace transforms of $y(t)$ and $u(t)$ respectively, and $z(s)$ is the Laplace transform of $z(t)$, which models the unknown bounded time-varying disturbances. The subsystem $\mathcal{G}_p$ has the input $u(t) = [u_1(t) \;\; u_2(t) \;\; u_3(t)]^\top$ issued from the outer loop and output $y(t) = [u_\theta(t) \;\; u_\psi(t) \;\; v(t)]^\top$, the input of subsystem $\mathcal{G}_e$. The subsystems $\mathcal{G}_e$ and $\mathcal{G}_p$ form the cascaded system shown in Fig. 7.

We note that $x(t)$ and $y(t)$ are the measured outputs of this cascaded system, and $u(t)$ is the only control signal. The maps f and g are known, while $G_p(s)$ is an unknown transfer function. The control objective is to stabilize $x(t)$ by the design of $u(t)$ without any modifications to the autopilot included in G_p. In that respect, we note that $\mathcal{G}_p$ can be described as

$$\mathcal{G}_p : \quad u_\theta(s) = G_{p1}(s)(u_1(s) + z_1(s)) \tag{28}$$
$$u_\psi(s) = G_{p2}(s)(u_2(s) + z_2(s)) \tag{29}$$
$$v(s) = G_{p3}(s)(u_3(s) + z_3(s))\,, \tag{30}$$

where $G_{p1}(s)$, $G_{p2}(s)$, $G_{p3}(s)$ are unknown stable transfer functions, $z_1(s)$, $z_2(s)$, $z_3(s)$ represent the Laplace transformation of some bounded time-varying disturbance signals $z_1(t)$, $z_2(t)$, $z_3(t)$, respectively. We note that the autopilot is designed to ensure that $y(t)$ tracks any smooth $u(t)$ in the absence of $\mathcal{G}_e$. We further assume that the time-varying disturbances $z_1(t), z_2(t), z_3(t)$ are bounded functions of time with uniformly bounded derivatives. That is,

$$|z_i(t)| \;\leq\; L_{i0}\,, \quad i = 1,2,3 \tag{31}$$
$$|\dot{z}_i(t)| \;\leq\; L_{i1}\,, \quad i = 1,2,3\,, \tag{32}$$

where L_{i0}, L_{i1} are some conservative known bounds.

Remark 2 *We notice that the bandwidth of the control channel of the closed-loop UAV with the autopilot is very limited, and the model (28) - (30) is valid only for low-frequency approximation of $\mathcal{G}_p$. Additionally, only very limited knowledge of the autopilot is assumed at this point. We do not assume knowledge of the state dimension of the unknown transfer functions $G_{pi}(s)$, $i = 1,2,3$. We only assume that these are strictly proper transfer functions.*

Next, we isolate the autopilot with the UAV to design an adaptive controller for it to track any desired bounded continuous reference input. Notice that since $u_{\theta_c}(t)$ and $u_{\psi_c}(t)$ stabilize the subsystem $\mathcal{G}_e$, the

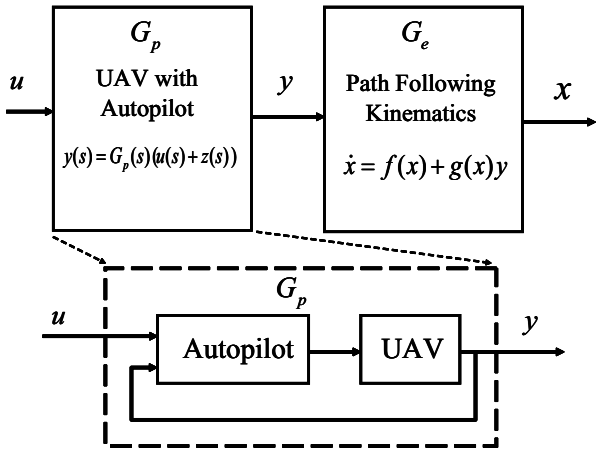

Figure 7. Cascaded systems

control objective for the subsystem $\mathcal{G}_p$ is reduced to designing an adaptive output feedback controller $u(t)$ such that the output $y(t) = [u_\theta(t)\ u_\psi(t)\ v(t)]^\top$ tracks the reference input $y_c(t) = [u_{\theta_c}(t)\ u_{\psi_c}(t)\ v_c(t)]^\top$ following a desired reference model, i.e.

$$u_\theta(s) \approx M(s)u_{\theta_c}(s) \tag{33}$$
$$u_\psi(s) \approx M(s)u_{\psi_c}(s) \tag{34}$$
$$v(s) \approx M(s)v_c(s)\,, \tag{35}$$

where the desired velocity command $v_c(t)$ will be specified in Section IV to achieve the coordination in time. In this paper, for simplicity we consider a first order system, by setting

$$M(s) = \frac{m}{s+m}\,, \quad m > 0. \tag{36}$$

Since the systems in (33), (34) and (35) have the same structure, we define the $\mathcal{L}_1$ adaptive control architecture only for the system in (33). The same design philosophy is true for the systems in (34) and (35). The elements of $\mathcal{L}_1$ adaptive controller for the system in (33) are presented next:

State Predictor: We consider the following state predictor:

$$\dot{\hat{u}}_\theta(t) = -m\hat{u}_\theta(t) + m\left(u_1(t) + \hat{\sigma}(t)\right), \quad \hat{u}_\theta(0) = 0\,, \tag{37}$$

where the adaptive estimate $\hat{\sigma}(t)$ is governed by the following adaptation law.

Adaptive Law: The adaptation of $\hat{\sigma}(t)$ is defined as:

$$\dot{\hat{\sigma}}(t) = \Gamma_c \mathrm{Proj}(\hat{\sigma}(t), -\tilde{u}_\theta(t)), \qquad \hat{\sigma}(0) = 0, \tag{38}$$

where $\tilde{u}_\theta(t) = \hat{u}_\theta(t) - u_\theta(t)$ is the error signal between the output of the system in (28) and the state predictor in (37), $\Gamma_c \in \mathbb{R}^+$ is the adaptation rate subject to a computable lower bound,[12] while Proj denotes the projection operator, which is performed on a compact set large enough to encompass the possible variation of uncertainties.[48] Quantitative analysis on the lower bound of Γ_c and other design details can be found in Ref.[12]

Control Law: The control signal is generated by:

$$u_1(s) = u_{\theta_c}(s) - C(s)\hat{\sigma}(s)\,, \tag{39}$$

where $C(s)$ is a strictly proper system with $C(0) = 1$, and $u_{\theta_c}(t)$ is the output of the stabilizing function in (17). In this paper, we consider the simplest choice of a first order low-pass filter:

$$C(s) = \frac{\omega}{s+\omega}\,. \tag{40}$$

The complete $\mathcal{L}_1$ adaptive controller consists of (37), (38) and (39) subject to the following $\mathcal{L}_1$-gain stability requirement introduced in Ref.[12]

$\mathcal{L}_1$-gain stability requirement: $C(s)$ and $M(s)$ need to ensure that

$$H(s) = \frac{G_{p1}(s)M(s)}{C(s)G_{p1}(s) + (1 - C(s))M(s)} \tag{41}$$

is stable and

$$\|G(s)\|_{\mathcal{L}_1} L_{z_1} < 1\,, \tag{42}$$

where

$$G(s) = H(s)(1 - C(s))\,, \tag{43}$$

and L_{z_1} is the Lipschitz constant of $z_1(t)$ w.r.t. $u_\theta(t)$.

Here, we note that we need to find suitable m and ω to stabilize $H(s)$ in (41). The condition in (42) is always satisfied for the system $\mathcal{G}_p$, since $z_1(t)$ does not depend on $u_\theta(t)$, which renders $L_{z_1} = 0$. In general, this may not be true.

III.B. Closed-loop Reference System

Consider the following closed-loop reference system:

$$\begin{aligned} u_{\theta_{ref}}(s) &= M(s)(u_{1_{ref}}(s) + \sigma_{ref}(s)), \\ \sigma_{ref}(s) &= \frac{(G_{p1}(s) - M(s))u_{1_{ref}}(s) + G_{p1}(s)z_1(s)}{M(s)} \\ u_{1_{ref}}(s) &= u_{\theta_c}(s) - C(s)\sigma_{ref}(s)\,. \end{aligned} \tag{44}$$

It follows from Ref.[12] that for any given $M(s)$ and $C(s)$, there exist constants $\gamma_{\theta_1} > 0$ and $\gamma_{u_1} > 0$ leading to the following result.

Lemma 2 *Given the system in (28) and the $\mathcal{L}_1$ adaptive controller defined via (37), (38) and (39) subject to (42), we have:*

$$\|u_\theta - u_{\theta_{ref}}\|_{\mathcal{L}_\infty} \leq \frac{\gamma_{\theta_1}}{\sqrt{\Gamma_c}}\,, \tag{45}$$

$$\|u_1 - u_{1_{ref}}\|_{\mathcal{L}_\infty} \leq \frac{\gamma_{u_1}}{\sqrt{\Gamma_c}}\,. \tag{46}$$

It follows from Lemma 2 that by increasing the adaptation rate Γ_c, we can render the bounds between the input/output signals of the closed-loop adaptive system and the reference system arbitrarily small.

III.C. Desired Low-pass system

Letting

$$y_{des}(s) = \begin{bmatrix} u_{\theta_{des}}(s) \\ u_{\psi_{des}}(s) \\ v_{des}(s) \end{bmatrix} = M(s)y_c(s)\,, \tag{47}$$

where $v_{des}(t)$ will follow from definition of $v_c(t)$ in the time-coordination step in Section IV, the performance bounds between the reference system in (44) and the low-pass system in (47) are given by the following lemma.

Lemma 3 *Given the system in (33) with the control signal in (28), we have:*

$$\|u_{\theta_{des}} - u_{\theta_{ref}}\|_{\mathcal{L}_\infty} \leq \gamma_{\theta_2}\,, \tag{48}$$

where

$$\gamma_{\theta_2} = \|H(s) - M(s)\|_{\mathcal{L}_1}\|u_{\theta_c}\|_{\mathcal{L}_\infty} + \|G(s)\|_{\mathcal{L}_1} L_{10}. \tag{49}$$

Proof. It follows from (44) that

$$u_{1_{ref}}(s) = u_{\theta_c}(s) - C(s)\frac{(G_{p1}(s) - M(s))u_{1_{ref}}(s) + G_{p1}(s)z_1(s)}{M(s)}\,,$$

and hence

$$u_{1_{ref}}(s) \;=\; \frac{M(s)u_{\theta_c}(s) - C(s)G_{p1}(s)z_1(s)}{C(s)G_{p1}(s) + (1 - C(s))M(s)}\,. \tag{50}$$

From (44), we have

$$u_{\theta_{ref}}(s) = G_{p1}(s)(u_{1_{ref}}(s) + z_1(s))\,. \tag{51}$$

Substituting (50) into (51), it follows from (41) that

$$\begin{aligned} u_{\theta_{ref}}(s) &= G_{p1}(s)\Big(\frac{M(s)u_{\theta_c}(s) - C(s)G_{p1}(s)z_1(s)}{C(s)G_{p1}(s) + (1 - C(s))M(s)} + z_1(s)\Big) \\ &= G_{p1}(s)M(s)\left(\frac{u_{\theta_c}(s) + (1 - C(s))z_1(s)}{C(s)G_{p1}(s) + (1 - C(s))M(s)}\right) \\ &= H(s)\left(u_{\theta_c}(s) + (1 - C(s))z_1(s)\right)\,. \end{aligned} \tag{52}$$

Using the definition in (47), we have

$$u_{\theta_{ref}}(s) - u_{\theta_{des}}(s) \;=\; (H(s) - M(s))u_{\theta_c}(s) + H(s)(1 - C(s))z_1(s)\,.$$

Assuming $H(s)$ is strictly proper and stable, it follows from (43) that $G(s)$ is also strictly proper and stable and hence

$$\|u_{\theta_{ref}} - u_{\theta_{des}}\|_{\mathcal{L}_\infty} \le \|H(s) - M(s)\|_{\mathcal{L}_1}\|u_{\theta_c}\|_{\mathcal{L}_\infty} + \|H(s)(1 - C(s))\|_{\mathcal{L}_1}\|z_1\|_{\mathcal{L}_\infty}\,. \tag{53}$$

Therefore, the relationship in (48) follows from (49) and (53), which proves the Lemma. □

Lemma 4 *Given the $\mathcal{L}_1$ adaptive controller defined via (37), (38) and (39) subject to (42), if*

$$|u_\theta(0) - u_{\theta_c}(0)| \le \frac{d_\theta}{m}\,, \tag{54}$$

where $d_\theta = \|\dot{u}_{\theta_c}\|_{\mathcal{L}_\infty}$, we have:

$$\|u_\theta - u_{\theta_c}\|_{\mathcal{L}_\infty} \;\le\; \gamma_\theta\,, \tag{55}$$

where $\gamma_\theta = \frac{\gamma_{\theta_1}}{\sqrt{\Gamma_c}} + \gamma_{\theta_2} + \frac{d_\theta}{m}$.

Proof. Let $u_{\theta_{ref}}(0) = u_{\theta_{des}}(0) = u_\theta(0)$. It follows from Lemmas 2 and 3 that

$$\|u_\theta - u_{\theta_{ref}}\|_{\mathcal{L}_\infty} + \|u_{\theta_{ref}} - u_{\theta_{des}}\|_{\mathcal{L}_\infty} \le \frac{\gamma_{\theta_1}}{\sqrt{\Gamma_c}} + \gamma_{\theta_2}\,. \tag{56}$$

Since $\dot{u}_{\theta_{des}} = -mu_{\theta_{des}} + mu_{\theta_c}$, we have

$$\dot{u}_{\theta_{des}} - \dot{u}_{\theta_c} = -m(u_{\theta_{des}} - u_{\theta_c}) + \dot{u}_{\theta_c}\,. \tag{57}$$

The bound on the initial error in (54) leads to

$$|u_{\theta_{des}}(t) - u_{\theta_c}(t)| \le \frac{d_\theta}{m}\,, \quad \forall\, t \ge 0\,. \tag{58}$$

A straightforward upper bounding

$$\|u_\theta - u_{\theta_c}\|_{\mathcal{L}_\infty} \;\le\; \|u_\theta - u_{\theta_{ref}}\|_{\mathcal{L}_\infty} + \|u_{\theta_{ref}} - u_{\theta_{des}}\|_{\mathcal{L}_\infty} + \|u_{\theta_{des}} - u_{\theta_c}\|_{\mathcal{L}_\infty}\,, \tag{59}$$

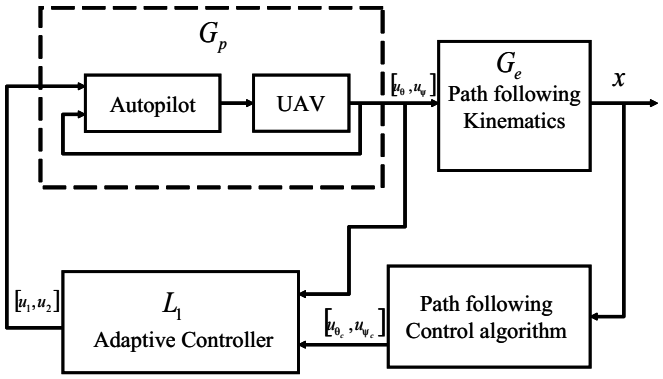

Figure 8. $\mathcal{L}_1$ **adaptive control of cascaded systems for path following**

leads to the claim in (55). □

Similarly, if we implement the $\mathcal{L}_1$ adaptive controller for the systems in (34) and (35), subject to

$$|u_\psi(0) - u_{\psi_c}(0)| \leq \frac{d_\psi}{m}, \tag{60}$$

$$|v(0) - v_c(0)| \leq \frac{d_v}{m}, \tag{61}$$

where $d_\psi = \|\dot{u}_{\psi_c}\|_{\mathcal{L}_\infty}$ and $d_v = \|\dot{v}_c\|_{\mathcal{L}_\infty}$, we can derive

$$\|u_\psi - u_{\psi_c}\|_{\mathcal{L}_\infty} \leq \gamma_\psi \tag{62}$$

$$\|v - v_c\|_{\mathcal{L}_\infty} \leq \gamma_v, \tag{63}$$

with $\gamma_\psi, \gamma_v > 0$ being constants similar to γ_θ. It we further want to reduce the bounds γ_θ, γ_ψ, γ_v, we need to choose m, ω and Γ_c large. It is straightforward to verify that

$$\lim_{\Gamma_c \to \infty} \left(\frac{\gamma_{\theta_1}}{\sqrt{\Gamma_c}} + \lim_{\omega \to \infty} \gamma_{\theta_2} \right) = 0 .$$

Since $u_{\theta_c}(t)$ is usually a low-pass signal with bounded derivative, γ_{θ_3} can be rendered arbitrarily small by increasing m. Hence, we have

$$\lim_{\Gamma_c \to \infty, m \to \infty} \left(\lim_{\omega \to \infty} \gamma_\theta \right) = 0 , \tag{64}$$

which is equally true for γ_ψ and γ_v.

III.D. Path-following with $\mathcal{L}_1$ Adaptive Augmentation

The cascaded closed-loop system defined via (17) (37), (38) and (39) is illustrated in Figure 8. We recall the main Theorem of Ref.[6] on stability of the cascaded system, which basically specifies the choice of the design constants in the $\mathcal{L}_1$ adaptive controller to ensure that the original domain of attraction for kinematic error equations given in (18) can be retained with $\mathcal{L}_1$ adaptive augmentation in the presence of a closed-loop UAV with the autopilot. Notice that the performance bounds for $\mathcal{L}_1$ adaptive controller above are computed for all three inputs to the autopilot (pitch rate, yaw rate and velocity), however due to the decoupling of space and time in the problem formulation, the path following problem is solved via pitch rate and yaw rate commands, therefore the stability proof below is pursued via the same Lyapunov function (19) independent of the velocity component. The latter will be addressed later in the paper in the context of time-critical coordination, where we will explicitly specify the desired velocity profile $v_c(t)$.

Lemma 5 *Given the cascaded controller defined via (17) (37), (38) and (39) subject to (14) and (16), if the initial conditions are bounded as in (54), (60), (61) and $x(0) \in \Omega$, where Ω is defined in (18), i.e.*

$$V_c(x(0)) \leq \frac{d^2}{2c_1}\,, \tag{65}$$

and m, ω and Γ_c verify

$$\gamma_\theta + \gamma_\psi \leq \frac{d\lambda_{\min}(Q)}{2\lambda_{\max}(P)}\sqrt{\frac{c_2}{c_1}}\,, \tag{66}$$

then $x(t) \in \Omega$ for all $t \geq 0$, i.e.

$$V_c(x(t)) \leq \frac{d^2}{2c_1}\,, \qquad \forall\ t \geq 0\,, \tag{67}$$

and the closed-loop system in (13) and (28) - (30) is ultimately bounded with the same bounds given in Lemma 1:

$$\begin{aligned} |x_F(t)| &\leq d\,, \qquad \forall\ t \geq 0\,, \\ |\theta_e(t)| &\leq \alpha\,, \qquad \forall\ t \geq 0\,, \\ |\psi_e(t)| &\leq \alpha\,, \qquad \forall\ t \geq 0\,, \end{aligned} \tag{68}$$

with α being defined in (16).

Proof. Using the same Lyapunov function as in (19) for the kinematic loop, it follows from (13) that

$$\begin{aligned} \dot{V}_c &= \frac{x_F}{c_1}(-\dot{l}(1-\kappa y_F) + v\cos(\theta_e)\cos(\psi_e)) + \frac{y_F}{c_1}(-\dot{l}(\kappa x_F - \zeta z_F) + v\cos(\theta_e)\sin(\psi_e)) + \frac{z_F}{c_1} \\ &\quad (-\zeta\dot{l}y_F - v\sin(\theta_e)) + \frac{\theta_e - \delta_\theta}{c_2}(u_\theta - \dot{\delta}_\theta) + \frac{\psi_e - \delta_\psi}{c_2}(u_\psi - \dot{\delta}_\psi) \\ &= \frac{x_F}{c_1}(-\dot{l}(1-\kappa y_F) + v\cos(\theta_e)\cos(\psi_e)) + \frac{y_F}{c_1}(-\dot{l}(\kappa x_F - \zeta z_F) + v\cos(\theta_e)\sin(\psi_e)) + \frac{z_F}{c_1} \\ &\quad (-\zeta\dot{l}y_F - v\sin(\theta_e)) + \frac{\theta_e - \delta_\theta}{c_2}(u_{\theta_c} - \dot{\delta}_\theta) + \frac{\psi_e - \delta_\psi}{c_2}(u_{\psi_c} - \dot{\delta}_\psi) \\ &\quad + \frac{\theta_e - \delta_\theta}{c_2}(u_\theta - u_{\theta_c}) + \frac{\psi_e - \delta_\psi}{c_3}(u_\psi - u_{\psi_c})\,, \end{aligned} \tag{69}$$

where we have taken into consideration the errors between u_θ and u_{θ_c}, u_ψ and u_{ψ_c}. From (15) we have

$$\dot{V}_c \leq -x^\top Q_c x + \frac{\theta_e - \delta_\theta}{c_2}(u_\theta - u_{\theta_c}) + \frac{\psi_e - \delta_\psi}{c_3}(u_\psi - u_{\psi_c})\,, \tag{70}$$

where Q_c is defined in (24). It follows from (55) and (62) that

$$\dot{V}_c \leq -x^\top Q_c x + \frac{|\theta_e - \delta_\theta|}{c_2}\gamma_\theta + \frac{|\psi_e - \delta_\psi|}{c_3}\gamma_\psi\,. \tag{71}$$

We prove (67) by contradiction. We note that $V_c(t)$ is continuous and differentiable. If (67) is not true, there exists t' such that

$$V_c(\tau) \leq \frac{d^2}{2c_1}\,, \qquad \forall\ \tau \in [0, t']\,, \tag{72}$$

$$V_c(t') = \frac{d^2}{2c_1}\,, \tag{73}$$

$$\dot{V}_c(t') > 0\,. \tag{74}$$

It follows from (72) that for any $\tau \in [0,\ t']$

$$
\begin{aligned}
|x_F(\tau)| &\leq d\,, && (75)\\
|y_F(\tau)| &\leq d\,,\\
|z_F(\tau)| &\leq d\,,\\
|\theta_e(\tau) - \delta_\theta(\tau)| &\leq \sqrt{c_2/c_1}d\,, && (76)\\
|\psi_e(\tau) - \delta_\psi(\tau)| &\leq \sqrt{c_2/c_1}d\,, && (77)\\
|\theta_e(\tau)| &\leq \sqrt{\frac{c_2 d^2}{c_1}} + \sup(\delta_\theta(\tau)) = \sqrt{\frac{c_2 d^2}{c_1}} + \sin^{-1}\left(\frac{d}{d_1+d}\right) = \alpha\,,\\
|\psi_e(\tau)| &\leq \sqrt{\frac{c_2 d^2}{c_1}} + \sup(\delta_\psi(\tau)) = \sqrt{\frac{c_2 d^2}{c_1}} + \sin^{-1}\left(\frac{d}{d_2+d}\right) = \alpha\,. && (78)
\end{aligned}
$$

The upper bound in (71) along with (76)-(77) leads to

$$\dot{V}_c(t') \leq -x^\top(t')Q_c x(t') + \frac{d}{\sqrt{c_1 c_2}}(\gamma_\theta + \gamma_\psi)\,. \tag{79}$$

Since

$$x^\top(t')Q_c x(t') \geq \frac{\lambda_{\min}(Q)}{\lambda_{\max}(P)}V(t')\,, \tag{80}$$

it follows from (73) that

$$x^\top(t')Q_c x(t') \geq \frac{d^2\lambda_{\min}(Q)}{2c_1\lambda_{\max}(P)}\,. \tag{81}$$

The design constraints in (66) lead to

$$\dot{V}_c(t') \leq 0\,, \tag{82}$$

which contradicts the assumption in (74). Hence, (67) holds. Since (72) leads to (75)-(78) for $\tau \in [0,\ t']$, the condition in (67) implies that (75)-(78) hold for all $t \geq 0$, and therefore the bounds in (68) hold. □

Remark 3 *The conditions on design constants in (66) can be satisfied by increasing m and ω as it follows from (64). Large m further requires ω and Γ_c be large. In practice, m and ω cannot be chosen arbitrarily large due to the limited bandwidth of the control channel of $\mathcal{G}_p$.*

Remark 4 *We notice that the above stability proof is different from common backstepping-type analysis for cascaded systems. The advantage of the above structure for the feedback design is that it retains the properties of the autopilot, which is designed to stabilize the inner-loop. As a result it leads to ultimate boundedness instead of asymptotic stability.*

IV. Time-Critical Coordination in the Absence of Autopilot

Having solved the complete path following problem for a single vehicle and an arbitrary speed profile, we now address the general problem of time-coordinated control of multiple vehicles. Examples of applications in which this would be useful include situations where all vehicles must arrive at their final destinations at exactly the same time, or at different times so as to meet a desired inter-vehicle arrival schedule. Without loss of generality, we consider the problem of simultaneous arrival. Let t_f be the arrival time of the first UAV. Denote l_{f_i} as the total length of the spatial path for i^{th} UAV. In addition, let $l_i(t)$ be the length from the origin to $P_i(t)$ along the spatial path of the i^{th} UAV. Define $l_i'(t) = l_i(t)/l_{fi}$. Clearly, $l_i'(t_f) = 1$ for $i = 1, 2, \ldots, n$ implies that all vehicles arrive at their final destination at the same time. Since $\dot{l}_i'(t) = \dot{l}_i(t)/l_{fi}$, it follows from (13) that

$$\dot{l}_i'(t) = \frac{K_1 x_{F_i}(t) + v_i(t)\cos\theta_{e,i}(t)\cos\psi_{e,i}(t)}{l_{fi}}\,, \tag{83}$$

where for simplicity we have kept K_1 without indexing. Following the same design philosophy, as we did for path following, we will first define the desired velocity profile $v_{c_i}(t)$ for the kinematics of the i^{th} UAV given by (83) to ensure that it achieves the time-critical coordination objective. Then using the same steps as in Section III we will rely on $u_3(t)$ to ensure that $v(t)$ can follow $v_c(t)$ according to a desired reference model $M(s)$. The desired velocity profile for each vehicle will be defined via dynamic inversion to achieve the time-coordination objective. Letting

$$u_{\text{coord}_i} = \frac{K_1 x_{F_i} + v_{c_i} \cos\theta_{e,i} \cos\psi_{e,i}}{l_{fi}}\,, \tag{84}$$

where u_{coord_i} is the i^{th} element of u_{coord}, it follows from (83) that the simplified coordination dynamics can be written as:

$$\dot{l'}(t) = u_{\text{coord}}(t)\,, \tag{85}$$

where $l' = [l'_1 \quad ...l'_n]^\top$ and $u_{\text{coord}} = [u_{\text{coord}_1} \quad ...u_{\text{coord}_n}]^\top$. Given a strategy for u_{coord}, the desired velocity profile for the i^{th} UAV can be computed as:

$$v_{c_i} = \frac{u_{\text{coord}_i} l_{fi} - K_1 x_{F_i}}{\cos\theta_{e,i} \cos\psi_{e,i}}\,, \quad i = 1, \cdots, n. \tag{86}$$

Thus, the coordination problem is reduced to defining $u_{\text{coord}}(t)$ such that $l'_i(t_f) = 1$ for $i = 1, 2, \ldots, n$. To account for the communication constraints, we borrow tools from algebraic graph theory (see for example Refs.[3,25]). To this effect, let L denote the Laplacian of a connected undirected graph Γ that captures the underlying bidirectional communication network of the UAV formation (in particular, the graph specifies for each vehicle what vehicles it exchanges information with). It is well known that $L \in \mathbb{R}^{n\times n}, L \geq 0$, $\text{rank}(L) = n-1$, and $L1_n = 0$.[3] Therefore, there exists a positive definite diagonal matrix L_d with the nonzero eigenvalues of L on the diagonal and an orthonormal matrix $U \in \mathbb{R}^{n\times(n-1)}, \text{rank}(U) = n-1$, such that

$$\begin{bmatrix} \frac{1_n}{\sqrt{n}} & U \end{bmatrix}^\top L \begin{bmatrix} \frac{1_n}{\sqrt{n}} & U \end{bmatrix} = \begin{bmatrix} 0 & 0 \\ 0 & L_d \end{bmatrix}, \tag{87}$$
$$U^\top 1_n = 0, U^\top U = \mathbb{I}, \text{ and } U L_d U^\top = L.$$

Motivated by the analysis in Ref.,[23] define the error vector

$$\mu(t) = U^\top l'(t). \tag{88}$$

It follows from $U^\top 1_n = 0$ that $\mu(t) = 0$ if and only if $l'_1(t) = l'_2(t) = \ldots = l'_n(t)$. This is well known in the literature on cooperative control as an Agreement Problem (see for example Refs.[28,19]). It follows from (85) and $U^\top U = \mathbb{I}$ that

$$\dot{\mu}(t) \quad = \quad U^\top u_{\text{coord}}(t). \tag{89}$$

Using this setup and considering the coordination system with simplified dynamics of (85), we impose that each UAV exchanges its coordination parameter $l'_i(t)$ with its neighbors according to the topology of the communications network, as expressed in terms of the connected undirected graph Γ. Elect vehicle 1 as the formation leader and let $v_{d,1}(t)$ denote its desired speed profile. We note that the desired arriving time of the all UAVs is then defined via $t_f = \frac{l_{f_1}}{v_{d,1}}$. The coordination problem is reduced to design of a control law for u_{coord} so that that $\mu(t_f) = 0$ for the dynamics in (89).

Remark 5 *The problem formulation above leads to an inherently finite time horizon problem for the dynamics in (89). In this paper, we solve it indirectly by using asymptotic analysis. Following a common practice, this can only be done approximately by judicious choice of the control gains and initial conditions. The solution to it is given below by Lemma 7, which is similar to the one in Ref.[44] for coordination of mobile robots.*

Let

$$\begin{aligned} u_{\text{coord}}(t) &= aLl'(t) + \begin{bmatrix} \frac{v_{d,1}(t)}{l_{f_1}} \\ \chi_I(t) \end{bmatrix} = C_1^\top \left(\frac{v_{d,1}(t)}{l_{f_1}} + aC_1 Ll'(t) \right) + C_2^\top (aC_2 Ll'(t) + \chi_I(t)) \\ \dot{\chi}_I(t) &= cC_2 Ll'(t), \end{aligned} \tag{90}$$

where a and c are negative scalars and

$$\begin{bmatrix} C_1 \\ C_2 \end{bmatrix} = \begin{bmatrix} 1 & 0_{n-1}^\top \\ 0_{n-1} & I_{(n-1)\times(n-1)} \end{bmatrix}. \tag{91}$$

The control law in (90) has a Proportional-Integral (PI) structure, thus allowing each vehicle to learn the speed of the leader, rather than having it available *a priori*. In fact, in scalar form the control law u_{coord} can be written as

$$\begin{aligned} u_{coord,1}(t) &= \frac{v_{d,1}(t)}{l_{f_1}} + \sum_{j \in J_1} a(l_1'(t) - l_j'(t)), \\ u_{coord,i}(t) &= \sum_{j \in J_i} a(l_i'(t) - l_j'(t)) + \chi_{I,i}(t), \\ \dot{\chi}_{I,i}(t) &= \sum_{j \in J_i} c(l_i'(t) - l_j'(t)), \quad i = 2, \ldots, n, \end{aligned} \tag{92}$$

where J_i denotes the set of neighboring vehicles that vehicle i is allowed to communicate with. Clearly, this implementation meets the communication constraints addressed in the coordination problem formulation. Notice also how the gains a and c play the role of tuning knobs to adjust the speed of convergence of the coordination error $\mu(t)$ to 0. This is important in light of the comments made in Remark 5.

The following Lemma will be useful for proving stability of (89) with (90).

Lemma 6 *Let A, B, C be positive definite matrices of compatible dimensions. Then the roots of* $\det(\lambda^2 A + B\lambda + C) = 0$ *have negative real parts.*

Proof. (By contradiction) Suppose it is not true. Then,

$$\text{Re}(\lambda) \geq 0. \tag{93}$$

Let $\lambda = \alpha + j\omega$, where $\alpha \geq 0$ and $\omega \geq 0$. Then there exists

$$p = p_r + p_i j \neq 0 \tag{94}$$

such that

$$\left((\alpha^2 - \omega^2)A + \alpha B + C\right) p_r - (2\alpha\omega A + B\omega) p_i = 0,$$

and

$$\left((\alpha^2 - \omega^2)A + \alpha B + C\right) p_i - (2\alpha\omega A + B\omega) p_r = 0,$$

which in turn implies that

$$p_i^\top (2\alpha A + B) p_i + p_r^\top (2\alpha A + B) p_r = 0. \tag{95}$$

Since A, B are positive definite and $\alpha \geq 0$, then $2\alpha A + B$ is positive definite. Hence, $p_i = p_r = 0$, which contradicts (94). Therefore, (93) is not true, and this completes the proof. □

The feedback system consisting of (89), (90) can be written as

$$\begin{aligned} \dot{\chi}_I &= cC_2 U L_d \mu \\ \dot{\mu} &= aL_d \mu + U^\top \left(C_1^\top \frac{v_{d,1}}{l_{f_1}} + C_2^\top \chi_I \right), \end{aligned} \tag{96}$$

where we have used the fact that $L = UL_dU^\top$. Let

$$x_v(t) = \begin{bmatrix} e_c(t) \\ \mu(t) \end{bmatrix}, \quad e_c(t) = \chi_I(t) - \frac{v_{d,1}(t)}{l_{f_1}} 1_{n-1}. \tag{97}$$

It follows from (96) that the coordination system can be rewritten as:

$$\dot{x}_v = \begin{bmatrix} 0 & cC_2UL_d \\ U^\top C_2^\top & aL_d \end{bmatrix} x_v + \begin{bmatrix} 0 \\ U^\top C_1^\top \frac{v_{d,1}}{l_{f_1}} + U^\top C_2^\top \frac{v_{d,1}}{l_{f_1}} 1_{n-1} \end{bmatrix}. \tag{98}$$

It follows from (91) that

$$C_2^\top 1_{n-1} + C_1^\top = 1_n \,. \tag{99}$$

Since $U^\top 1_n = 0$ (see (87)), we have

$$U^\top C_1^\top \frac{v_{d,1}}{l_{f_1}} + U^\top C_2^\top \frac{v_{d,1}}{l_{f_1}} 1_{n-1} = 0 \,,$$

and hence (98) can be rewritten as:

$$\dot{x}_v = \begin{bmatrix} 0 & cC_2UL_d \\ U^\top C_2^\top & aL_d \end{bmatrix} x_v \,. \tag{100}$$

The next Lemma follows directly from Ref.,[30] which ensures that $\mu = 0$ is an exponentially stable origin for the system in (89) with (90).

Lemma 7 *The control law in (90) solves the coordination problem for the dynamics in (89).*

Proof. First we prove that the matrix $C_2U \in \mathbb{R}^{(n-1)\times(n-1)}$ has rank $n-1$. From the definition of C_2, it follows that C_2U consists of the last $n-1$ rows of U. Suppose there exists a vector, $\bar{x}$ such that $\bar{x}^\top C_2U = 0$. Let $\bar{x}_1 = [0 \;\; \bar{x}^\top]^\top$. Since $\bar{x}^\top C_2 = \bar{x}_1^\top$, we obtain that $\bar{x}_1^\top U = 0$, which contradicts the fact that $1_n^\top U = 0$ and 1_n is the only element in the kernel of U (see (87)).

Next, we compute the eigenvalues of the state matrix associated with (109) as the solutions of

$$\det \begin{bmatrix} \lambda\mathbb{I} & -cC_2UL_d \\ -U^\top C_2^\top & \lambda\mathbb{I} - aL_d \end{bmatrix} = 0 \tag{101}$$

leading to

$$\det(\lambda\mathbb{I}(\lambda\mathbb{I} - aL_d) - cU^\top C_2^\top C_2UL_d) = \det(\lambda^2 L_d^{-1} - a\lambda\mathbb{I} - cU^\top C_2^\top C_2U) = 0.$$

In the last step we have exploited the fact that for any compatible square matrices A, B, C, D

$$\det \begin{bmatrix} A & B \\ C & D \end{bmatrix} = \det(AD - CB) \tag{102}$$

if $AC = CA$.[27] Since C_2U is full rank, $U^\top C_2^\top C_2U$ is positive definite. It now follows from Lemma 6 that the roots λ in (101) have negative real parts for any negative scalar gains a and c, thus proving stability. □

V. $\mathcal{L}_1$ Adaptive Augmentation of the Velocity Loop for Time-Critical Coordination in the Presence of Autopilot

Recall that in Section III we defined the $\mathcal{L}_1$ adaptive augmentation for all three inputs to the autopilot: pitch rate $u_{\theta_c}(t)$, yaw rate $u_{\psi_c}(t)$ and velocity $v_c(t)$, but we proceeded only with analysis of the pitch rate,

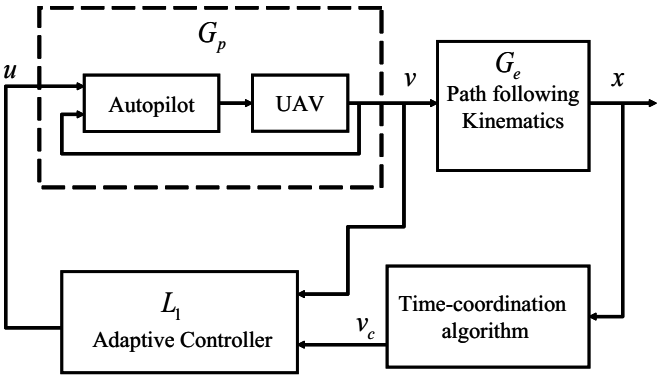

Figure 9. $\mathcal{L}_1$ **adaptive control of cascaded systems for coordination**

acknowledging that the other two are the same. We further pursued the stability of cascaded system in Section III.D in the context of path following problem without any regard to the velocity component. In this section, we pursue the stability analysis of the coordination dynamics in the presence of velocity error, Fig. 9. Recall that the signal $u_3(t)$ designed for (30) leads to $v(t)$, for which the desired control objective is stated in (35) with $v_c(t)$ being defined in (86). Letting

$$\tilde{v}_i(t) = v_{c_i}(t) - v_i(t), \quad i = 1, \cdots, n\,, \tag{103}$$

denote the velocity error for the i^{th} vehicle in the coordination, if the upper bound on the initial condition in (61) holds, it follows from (63) that

$$\|\tilde{v}_i\|_{\mathcal{L}_\infty} \leq \gamma_{v_i}\,, \qquad i = 1, .., n\,. \tag{104}$$

In this section, we analyze the performance of the coordination dynamics in the presence of this error. The kinematic equation in (83) can be rewritten as:

$$\dot{l}_i'(t) = u_{\text{coord}_i}(t) + \frac{\tilde{v}_i(t)\cos\theta_{e,i}(t)\cos\psi_{e,i}(t)}{l_{fi}}\,. \tag{105}$$

Then the coordination dynamics in (89) take the form:

$$\dot{\mu}(t) \;\; = \;\; U^\top u_{\text{coord}}(t) + U^\top \varphi(t)\,, \tag{106}$$

where $\varphi(t) \in \mathbb{R}^n$ is a vector with its i^{th} element $\frac{\tilde{v}_i(t)\cos\theta_{e,i}(t)\cos\psi_{e,i}(t)}{l_{fi}}$, and therefore the closed-loop coordination system (96) can be written as

$$\begin{aligned} \dot{\chi}_I &= cC_2UL_d\mu \\ \dot{\mu} &= aL_d\mu + U^\top\left(C_1^\top\frac{v_{d,1}}{l_{f_1}} + C_2^\top\chi_I\right) + U^\top\varphi. \end{aligned} \tag{107}$$

It follows from (107) that the coordination system can be rewritten as:

$$\dot{x}_v = \begin{bmatrix} 0 & cC_2UL_d \\ U^\top C_2^\top & aL_d \end{bmatrix} x_v + \begin{bmatrix} 0 \\ U^\top\varphi \end{bmatrix} + \begin{bmatrix} 0 \\ U^\top C_1^\top\frac{v_{d,1}}{l_{f_1}} + U^\top C_2^\top\frac{v_{d,1}}{l_{f_1}}1_{n-1} \end{bmatrix}, \tag{108}$$

and hence (108) can be rewritten as:

$$\dot{x}_v = \begin{bmatrix} 0 & cC_2UL_d \\ U^\top C_2^\top & aL_d \end{bmatrix} x_v + \begin{bmatrix} 0 \\ U^\top\varphi \end{bmatrix}. \tag{109}$$

We note that Lemma 7 implies that $\begin{bmatrix} 0 & cC_2L_d \\ U^\top C_2^\top & aL_d \end{bmatrix}$ is Hurwitz. Hence, there exists symmetric positive definite matrix P_e which solves the following Lyapunov equation

$$\begin{bmatrix} 0 & cC_2L_d \\ U^\top C_2^\top & aL_d \end{bmatrix}^\top P_e + P_e \begin{bmatrix} 0 & cC_2L_d \\ U^\top C_2^\top & aL_d \end{bmatrix} = -Q_e, \tag{110}$$

where $Q_e \in \mathbb{R}^{2(n-1)\times 2(n-1)}$ is a positive semi-definite matrix. Since $|\cos\theta_{e,i}\cos\psi_{e,i}| \leq 1$, it follows from (104) and the upper bound on initial condition in (61) that there exists constant $k_v > 0$ such that

$$\left\| P_e \begin{bmatrix} 0 \\ U^\top \varphi \end{bmatrix} \right\| \leq k_v \gamma_v \,, \tag{111}$$

where $\gamma_v = \max\{\gamma_{v_1}, \cdots, \gamma_{v_n}\}$.

Lemma 8 *Let $V_e(t) = x_v^\top(t) P_e x_v(t)$. Suppose that the upper bound on initial condition in (61) holds for all vehicles*

$$|v_i(0) - v_{c_i}(0)| \leq \frac{d_v}{m} \,, \quad i = 1, \cdots, n \,,$$

and

$$V_e(0) > \lambda_{\max}(P_e) \left(\frac{2k_v\gamma_v}{\lambda_{\min}(Q_e)} \right)^2 . \tag{112}$$

Then

$$V_e(t) \leq V_e(0) \,, \quad \forall\ t \geq 0 \,, \tag{113}$$

and the system in (109) is ultimately bounded.

Proof. It follows from (109) and (110) and the definition of φ that

$$\dot{V}_e \leq x_v^\top Q_e x_v + 2x_v^\top P_e \begin{bmatrix} 0 \\ U^\top \varphi \end{bmatrix} . \tag{114}$$

Using the upper bound from (111) we have

$$\dot{V}_e(t) \leq -x_v^\top(t) Q_e x_v(t) + 2k_v\gamma_v \|x_v(t)\| \,. \tag{115}$$

We note that $V_e(t)$ is continuous. For any $t' \geq 0$ such that

$$V_e(t') = V_e(0) \,, \tag{116}$$

it follows from (112) that

$$V_e(t') \geq \lambda_{\max}(P_e) \left(\frac{2k_v\gamma_v}{\lambda_{\min}(Q_e)} \right)^2 . \tag{117}$$

Since $V_e(t') \leq \lambda_{\max}(P_e)\|x_v(t')\|^2$, it follows from (117) that

$$\|x_v(t')\| \geq \frac{2k_v\gamma_v}{\lambda_{\min}(Q_e)} \,. \tag{118}$$

It follows from (115) and (118) that

$$\dot{V}_e(t') \leq -\lambda_{\min}(Q_e)\|x_v(t')\|^2 + 2k_v\gamma_v\|x_v(t')\| \leq 0 \,, \tag{119}$$

which implies that $V(t)$ cannot exceed $V_e(0)$. This completes the proof. □

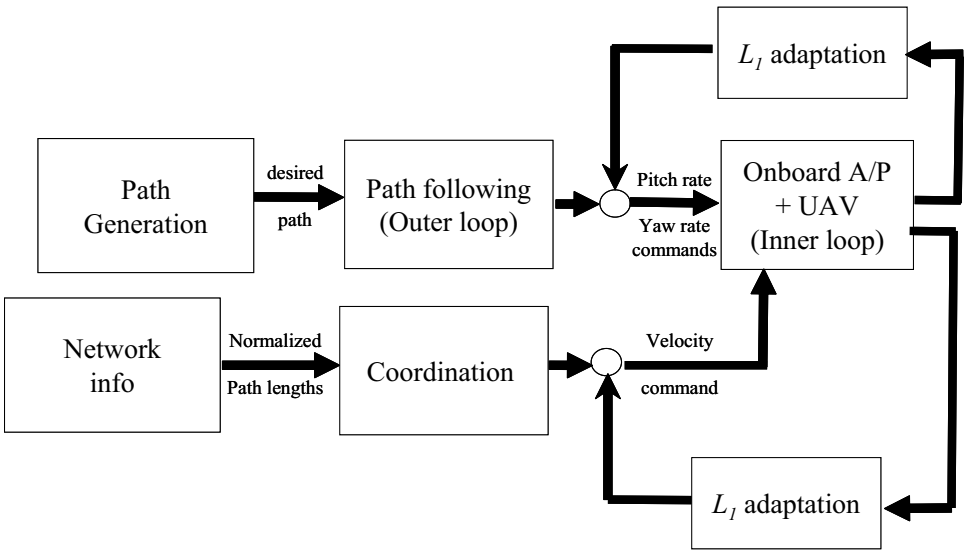

Figure 10. Coordinated path following

VI. Combined Path Following and Time Critical Coordination with $\mathcal{L}_1$ Adaptive Augmentation

The complete architecture of coordinated path following is presented in Fig. 10, the stability of which we prove in this section.

First we notice that from $L = UL_dU^\top$ in (87), (88) and (90) it follows that

$$u_{\text{coord}}(t) = aUL_dU^\top l'(t) + \begin{bmatrix} \frac{v_{d,1}(t)}{l_{f_1}} \\ \chi_I(t) \end{bmatrix} = aUL_d\mu(t) + \begin{bmatrix} \frac{v_{d,1}(t)}{l_{f_1}} \\ \chi_I(t) \end{bmatrix}. \tag{120}$$

Since (91) and (97) imply that

$$\begin{bmatrix} \frac{v_{d,1}(t)}{l_{f_1}} \\ \chi_I(t) \end{bmatrix} = \begin{bmatrix} \frac{v_{d,1}(t)}{l_{f_1}} \\ e_c(t) + \frac{v_{d,1}(t)}{l_{f_1}} 1_{n-1} \end{bmatrix} = C_2^\top e_c(t) + \frac{v_{d,1}(t)}{l_{f_1}} 1_n\,, \tag{121}$$

it follows from the definition of C_v in (129) and (120) that

$$u_{\text{coord}}(t) = C_v x_v(t) + \frac{v_{d,1}(t)}{l_{f_1}} 1_n\,. \tag{122}$$

Since

$$\|C_v x_v(t)\|^2 \leq \frac{\lambda_{\max}(C_v^\top C_v)}{\lambda_{\min}(P_e)} V_e(t)\,, \tag{123}$$

we have

$$\|C_v x_v(t)\| \leq \sqrt{\frac{\lambda_{\max}(C_v^\top C_v)}{\lambda_{\min}(P_e)} V_e(t)}\,, \tag{124}$$

and hence

$$\|y_{v_i}(t)\| \leq \sqrt{\frac{\lambda_{\max}(C_v^\top C_v)}{\lambda_{\min}(P_e)} V_e(t)}\,, \tag{125}$$

where y_{v_i} is the i^{th} element of $C_v x_v(t)$.

First we will prove that the resulting velocity for the i^{th} UAV verifies the *a priori* specified lower bound:

$$v_i \geq v_{\min}\,. \tag{126}$$

Next we show that the entire closed-loop system, which consists of kinematic path-following, time-critical coordination and $\mathcal{L}_1$ adaptive augmentation for both loops, is stable. The main result of this paper is stated next.

Theorem 1 *Let $\bar{V}_e$ be the upper bound*

$$\lambda_{\max}(P_e)\left(\frac{2k_v\gamma_v}{\lambda_{\min}(Q_e)}\right)^2 \leq \bar{V}_e\,, \tag{127}$$

while c_1, c_2, d, γ_v verify the condition in (16) in addition to

$$\frac{\left(\frac{v_{d,1}}{l_{f_1}} - \sqrt{\frac{\lambda_{\max}(C_v^\top C_v)}{\lambda_{\min}(P_e)}\bar{V}_e}\right) l_{fi} - K_1 d}{\cos^2\alpha} > v_{\min} + \gamma_{v_i}\,, \quad i = 1,..,n\,, \tag{128}$$

where $v_{\min}$ is the lower bound (126),

$$C_v = \begin{bmatrix} aUL_d & C_2^\top \end{bmatrix}\,, \tag{129}$$

and let m, ω and Γ_c in the design of $\mathcal{L}_1$ adaptive controller be chosen to verify

$$\gamma_{\theta_i} + \gamma_{\psi_i} \leq \frac{d\lambda_{\min}(Q)}{2\lambda_{\max}(P)}\sqrt{\frac{c_2}{c_1}}\,, \quad i = 1,\cdots,n. \tag{130}$$

If the initial condition for the Lyapunov function of the i^{th} vehicle is constrained to its domain of attraction, defined via (18):

$$V_{c_i}(0) \;\leq\; \frac{d^2}{2c_1}\,, \qquad i = 1,\cdots,n\,, \tag{131}$$

and in addition to (54), (60), (61) one has

$$V_e(0) \;\leq\; \bar{V}_e\,, \tag{132}$$

then

$$\begin{aligned} V_{c_i}(t) &\leq \frac{d^2}{2c_1}\,, \quad \forall\, t \geq 0\,, \quad i = 1,..,n\,,\\ V_e(t) &\leq \bar{V}_e\,, \quad \forall\, t \geq 0\,, \end{aligned} \tag{133}$$

implying that the entire system is ultimately bounded.

Proof. At first we will prove

$$v_i(t) > v_{\min}, \quad \forall\, t \geq 0\,, \quad i = 1,..,n\,. \tag{134}$$

If (134) is not true, since $v_i(0) > v_{\min}$ and $v_i(t)$ is continuous, there exists τ and a vehicle, $j \in \{1,\ldots,n\}$, such that

$$v_j(\tau) = v_{\min}. \tag{135}$$

In addition, we have

$$v_i(t) \geq v_{\min}, \quad \forall\, t \in [0,\tau]\,, \quad i = 1,..,n\,. \tag{136}$$

Since (130), (131) and (136) verify the condition of Lemma 5, it follows that for all $i = 1,\cdots,n$

$$\begin{aligned} |x_{F_i}(t)| &\leq d\,, \quad \forall\, t \in [0,\tau]\,,\\ |\theta_{e_i}(t)| &\leq \alpha\,, \quad \forall\, t \in [0,\tau]\,,\\ |\psi_{e_i}(t)| &\leq \alpha\,, \quad \forall\, t \in [0,\tau]\,. \end{aligned} \tag{137}$$

Since the results of Lemma 8 hold independent of path following, it follows from (127), (132) that

$$V_e(t) \leq \bar{V}_e\,, \qquad \forall\, t \geq 0\,. \tag{138}$$

It follows from (125) and (138) that

$$\|y_{v_i}(t)\| \leq \sqrt{\frac{\lambda_{\max}(C_v^\top C_v)}{\lambda_{\min}(P_e)}\bar{V}_e}\,, \tag{139}$$

Hence, it follows form (122) that

$$|u_{\text{coord}_i}(t)| \geq \frac{v_{d,1}(t)}{l_{f_1}} - \sqrt{\frac{\lambda_{\max}(C_v^\top C_v)}{\lambda_{\min}(P_e)}\bar{V}_e}\,, \qquad \forall\, t \geq 0\,. \tag{140}$$

Thus, (86) implies

$$v_{c_i} \geq \frac{\left(\frac{v_{d,1}}{l_{f_1}} - \sqrt{\frac{\lambda_{\max}(C_v^\top C_v)}{\lambda_{\min}(P_e)}\bar{V}_e}\right) l_{fi} - K_1 x_{F_i}}{\cos\theta_{e,i}\cos\psi_{e,i}}\,. \tag{141}$$

It follows from (137) and (141) that

$$v_{c_i}(t) \geq \frac{\left(\frac{v_{d,1}}{l_{f_1}} - \sqrt{\frac{\lambda_{\max}(C_v^\top C_v)}{\lambda_{\min}(P_e)}\bar{V}_e}\right) l_{fi} - K_1 d}{\cos^2\alpha}\,, \quad t \in [0,\ \tau]\,, \quad i = 1,..,n\,. \tag{142}$$

From (104) and (128) it follows that

$$v_i(t) \geq v_{c_i}(t) - \gamma_{v_i} > v_{\min}\,, \qquad \forall\ t\ \in\ [0,\ \tau]\,, \quad i = 1,..,n\,, \tag{143}$$

which contradicts (135). Therefore, (134) holds. If (134) is true, it can be verified easily that the conditions of Lemmas 1 and 8 are verified for any $t \geq 0$, and (133) is proved. □

In case of exact tracking of $v_i(t)$, $u_{\theta_i}(t)$, $u_{\psi_i}(t)$ of their commands $v_{c_i}(t)$, $u_{\theta_{c_i}}(t)$, $u_{\psi_{c_i}}(t)$, $i = 1,..,n$, we have

$$\gamma_{\theta_i} = 0\,, \qquad \gamma_{\psi_i} = 0\,, \qquad \gamma_{v_i} = 0\,, \qquad i = 1,..,n. \tag{144}$$

The following corollary can be proved straightforwardly.

Corollary 1 *If c_1, c_2, d and $\bar{V}_e$ verify (16) in addition to*

$$\frac{\left(\frac{v_{d,1}}{l_{f_1}} - \sqrt{\frac{\lambda_{\max}(C_v^\top C_v)}{\lambda_{\min}(P_e)}\bar{V}_e}\right) l_{fi} - K_1 d}{\cos^2\alpha} > v_{\min}\,, \tag{145}$$

and

$$V_{c_i}(0) \leq \frac{d^2}{2c_1}\,, \tag{146}$$

$$V_e(0) \leq \bar{V}_e\,, \tag{147}$$

then

$$\begin{aligned} V_{c_i}(t) &\leq \frac{d^2}{2c_1}\,, \quad \forall\, t \geq 0, \\ V_e(t) &\leq \bar{V}_e\,, \quad \text{`}\forall\, t \geq 0\,, \end{aligned} \tag{148}$$

and the entire system is ultimately bounded.

The proof of Corollary 1 follows from Theorem 1 immediately. We note that (145) can always be satisfied by choosing d and $\bar{V}_e$ small enough.

VII. Hardware in-the-Loop Setup and Experimental Results

The complete path following control system with adaptation for a single UAV, shown in Figure 8, was implemented on an experimental UAV Rascal operated by NPS. The Hardware In The Loop (HITL) and flight test setups[30] are shown in Fig. 11; note that both configurations are identical except the sensor data is software generated in the HITL simulation.

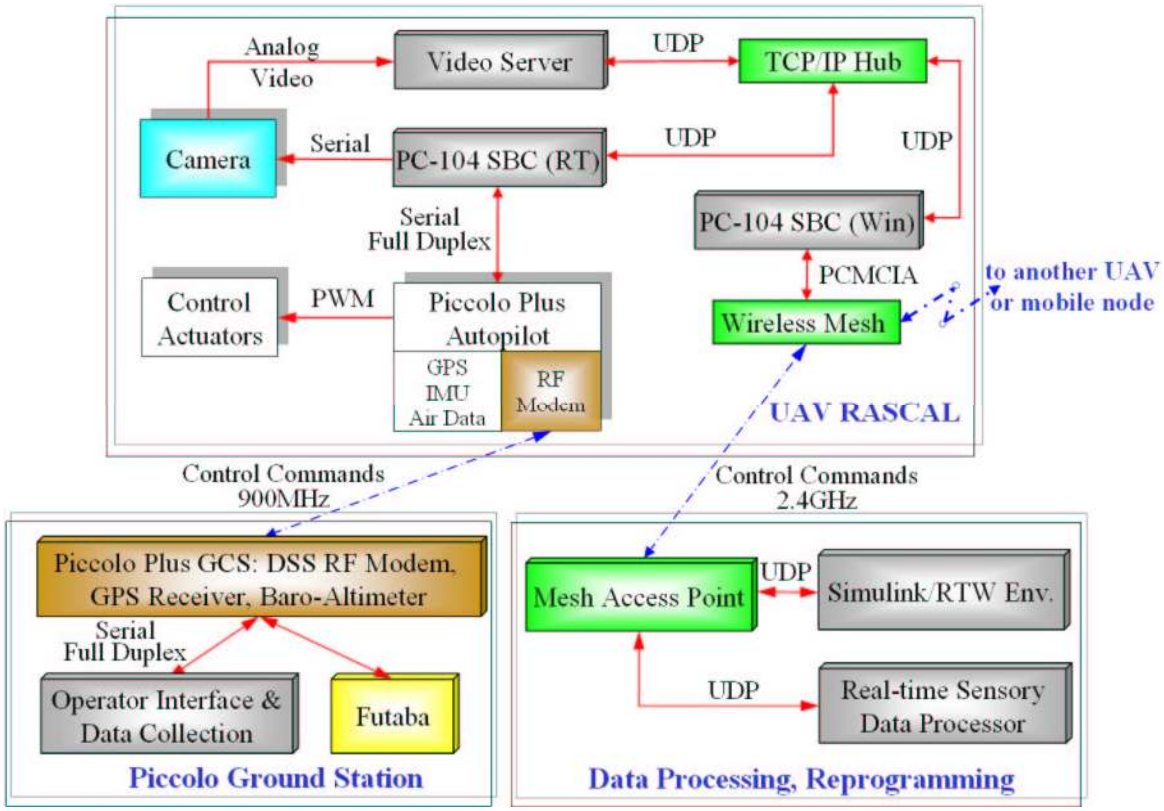

Figure 11. Avionics architecture including two embedded processors and an AP

Customized RASCAL model aircraft were used for the experimental part of the work (Fig.12). Payload bay of each aircraft is used to house two PC104 embedded computers assembled in a stack, wireless network link, and the Piccolo autopilot[47] with its dedicated control channel. The first PC-104 board (see SBC (RT) in Fig. 11) runs developed algorithms in real-time while directly communicating with the autopilot (AP) over the serial link. The second PC-104 computer (see SBC (Win) in Fig. 11) is equipped with a mesh network card (Motorola WMC6300 Mesh Card) that provides wireless communication to another UAV as well as to the data processing center on the ground. This second computer performs software bridging of onboard wired and external wireless mesh networks. Thus, direct connection with the onboard autopilot efficiently eliminates communication delays between the high-level control algorithm and the autopilot. In turn, an integration of the self-configuring wireless mesh network allows for transparent inter-vehicle communication making it suitable for coordination in time.

In order to provide data for the qualitative analysis of the developed path following and coordination algorithms, the onboard avionics has also been equipped with the capability to store critical data in real time into the onboard solid state memory disk (see SSD in Fig. 11). The autopilot telemetry information including spatial attitude, rates and the inertial speed is logged with 20 Hz sampling rate, while the positional data is logged at 1Hz frequency; they are the highest possible rates delivered by the autopilot. Internal data of the path following-coordination and adaptation algorithms is logged with 100Hz sampling rate. In addition, some limited data is transmitted to the ground while in flight. This allows for online estimation of the algorithms performance and control gains tuning. The key element of this architecture is that the standard

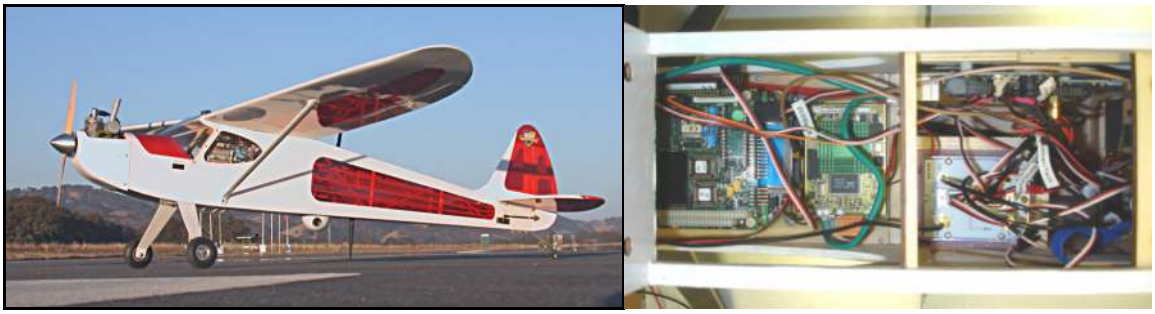

Figure 12. RASCAL UAV and its payload bay with the custom built avionics

Piccolo GCS retains full authority control over the autopilot at each stage of the flight, thereby securing the flight operation. When the AP is in the autonomous mode, the onboard segment receives commands over the mesh network from either the data processing segment, the collaborating small UAV (SUAV) or any other mesh-enabled PC. The standard GCS command and control link with AP allows monitoring the correctness of the flight operation through the pre-built functionality of the Operator Interface (OI) software that comes with the Piccolo AP. The control response provided by the UAV under the AP control is transmitted to the GCS, where they are available for continuous analysis. Should a "glitch" in the new control algorithm, AP behavior, SUAV dynamics or communication occur, the safety of the flight is not compromised. A pre-built set of AP safety limits immediately detects this, displays particular warning or even automatically regains control of the SUAV, thus returning it to safe conditions.

Based on the presented hardware setup, the cascaded controller defined in (17), (37), (38), and (39) with $M(s) = \frac{1}{10s+1}, C(s) = \frac{1}{10s+1}$, and $\Gamma = 10$ was flight tested in February 2007. The subsystem $\mathcal{G}_p$ represents the Rascal with the Piccolo autopilot as described in Ref.[30] Figure 13 shows how the developed system was used for the flight testing of the path following/adaptation/coordination algorithms running onboard in real-time; a collective picture of 15 trials obtained during just one flight test is presented. As for the coordination, the speed of virtual cooperative UAV was simulated to be constant. In this picture, the red trajectories represent the required/commanded flight path and the blue one shows the actual flight path of the UAV. Each trial was used to tune the control law parameters in order to achieve more accurate path following and coordination. Having been transmitted to the ground while in flight, these trajectories, as well as the control commands with the AP responses, allow for rapid evaluation and adjustment of the control performance.

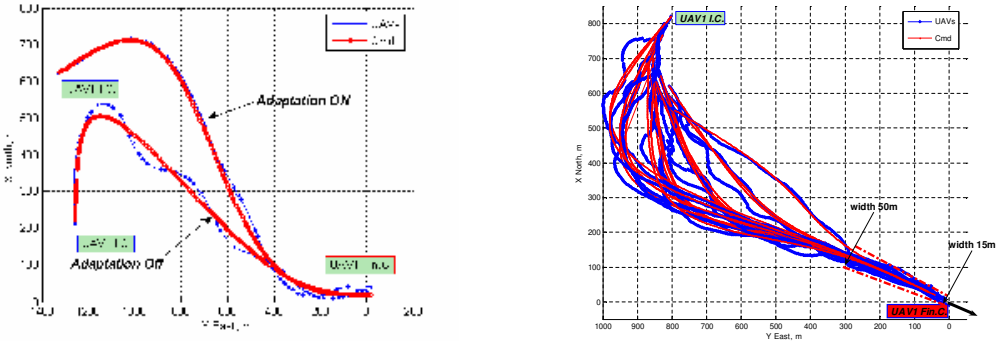

Figure 13. Performance comparison with and without $\mathcal{L}_1$ adaptation (left) and 3D path following in the autonomous landing scenario (right)

Figure 14(a) presents one of the trials of Fig.13 in details; it shows the inertial position of UAV with respect to the commanded feasible trajectory generated online as introduced in Section II. Figure 14(a) also shows the corresponding rate commands of the autopilot as well as errors of the UAV tracking the trajectory. It can be seen that the maximum deviation from the desired trajectory is about $40m$, which corresponds to

the point of the sharp turn. Other than at this point, the tracking errors are very small and the UAV is following the commanded path very closely.

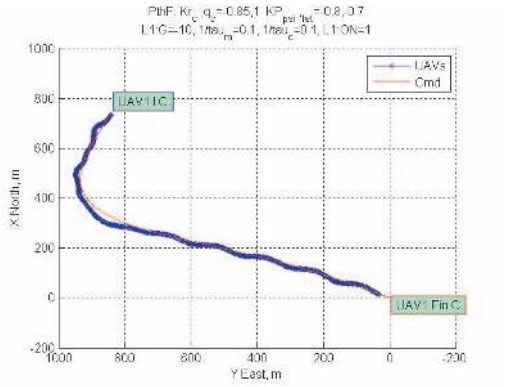

(a) Desired (red) and actual (blue) UAV trajectories from flight test with $\mathcal{L}_1$ adaptive controller

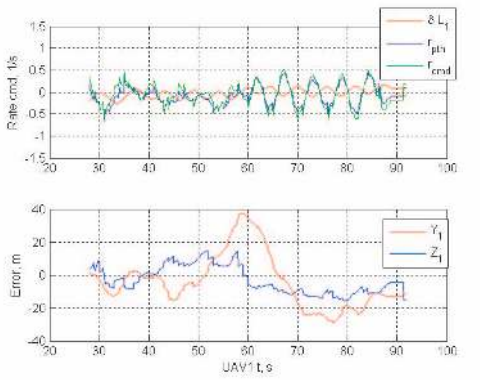

(b) Top: path following turn rate command and contributions from outer loop and $\mathcal{L}_1$ adaptation. Bottom: path following errors

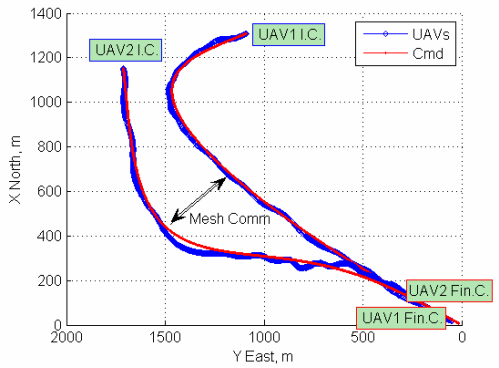

(c) Simultaneous arrival of two UAVs to the same terminal conditions (separated by altitude).

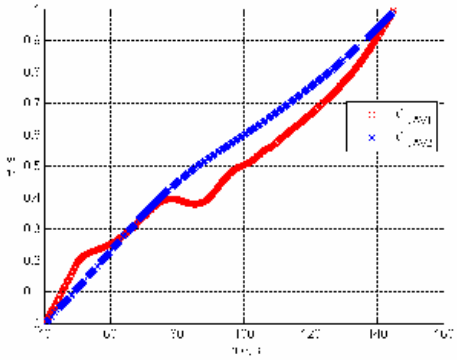

(d) Coordination states for each UAV.

Figure 14. Flight Test Results (top) and Hardware-in-the-Loop Simulations (bottom)

Figures 14(c) - 14(d) include results of an HITL test where two UAVs follow feasible trajectories while using their velocities to coordinate simultaneous arrival at their respective terminal conditions. Results of Figure 14(c) show the desired and the actual paths of each UAV. Control commands and errors for both UAVs are similar to the results of one UAV tracking the path. As in the case of one UAV, the control efforts required to bring each airplane to the commanded trajectory do not exceed any limitations imposed by the autopilot and are typical for this class of UAVs. Finally, normalized coordination states for each UAV are presented in Figure 14(d); two graphs represent coordination efforts required to deliver two UAVs to the terminal conditions at the same time. Both airplanes arrive at the final position at nearly the same time.

The results presented above demonstrate feasibility of the onboard integration of the path following, adaptation and coordination concepts. During the flight experiments, the required control commands (including adaptive contribution) have never exceeded the limits defined for the UAV in traditional waypoint navigation mode. At the same time the achieved functionality of the UAV following 3D curves in inertial space has never been available for the airplanes equipped with traditional AP; adaptive concept explicitly outperforms the conventional waypoint navigation method. Presented results not only demonstrate the

feasibility of the concept but provide a roadmap for further development and onboard implementation of intelligent multi-UAV coordination.

VIII. Conclusion

A novel solution was presented to the problem of coordinated control of multiple unmanned air vehicles (UAVs) that ensures collision-free maneuvers under strict spatial and temporal constraints. The theoretical framework adopted includes algorithms for deconflicted real-time path generation, nonlinear path following, and multiple vehicle coordination. Path following led to a classical inner-outer structure that relies on the augmentation of existing autopilots with $\mathcal{L}_1$ adaptive output feedback control laws. Multiple vehicle coordinated control was done by adjusting the speed profiles of the vehicles along their paths in response to information exchanged over the underlying communication network. The $\mathcal{L}_1$ adaptive control was once again used to yield an inner-outer loop structure for vehicle coordination with guaranteed performance bounds.

Both theoretical and flight test results were presented. Simulations showed the efficacy of the path following and time-critical coordination algorithms. Flight test results obtained at Camp Roberts, CA in 2007 proved that the algorithm for path generation lends itself to real-time implementation and yields feasible trajectories that meet prescribed conditions. The experimental results were also instrumental in demonstrating the benefits of using $\mathcal{L}_1$ adaptive control loops for path following of single vehicle by resorting to an inner-outer loop control structure and coordination of two vehicles over fixed communication network topology. Future work will extend the framework to time-varying network topologies, including network failures and time-delays.

References

[1]J. Baillieul and A. Suri. Information Patterns and Hedging Brockett's Theorem in Controlling Vehicle Formations *In Proceedings of IEEE Conference on Decision and Control*, Maui, Hawaii, 2003.

[2]R. Beard, C. Cao and N. Hovakimyan. An $\mathcal{L}_1$ Adaptive Pitch Controller for Miniature Air Vehicles. *In Proceedings of AIAA Guidance, Navigation, and Controls Conference,* Keystone, CO, 2006.

[3]N. Biggs. *Algebraic Graph Theory* Cambridge University Press, 1993.

[4]S. Boyd, L. El Ghaoui, E. Feron, and V. Balakrishnan. Linear Matrix Inequalities in System and Control Theory. *SIAM*, 1994.

[5]C. Cao, N. Hovakimyan and E. Lavretsky. Application of $\mathcal{L}_1$ Adaptive Controller to Wing Rock. *In Proceedings of AIAA Guidance, Navigation, and Controls Conference,* Keystone, CO, 2006.

[6]C. Cao, N. Hovakimyan, I. Kaminer, V. Patel and V. Dobrokhodov. Stabilization of Cascaded Systems via $\mathcal{L}_1$ Adaptive Controller with Application to a UAV Path Following Problem and Flight Test Results. *In Proceedings of American Control Conference*, New York, NY, 2007.

[7]C. Cao and N. Hovakimyan. Design and Analysis of a Novel $\mathcal{L}_1$ Adaptive Controller, Part I: Control Signal and Asymptotic Stability. *In Proceedings of American Control Conference*, pp. 3397 - 3402, Minneapolis, MN, 2006.

[8]C. Cao and N. Hovakimyan. Design and Analysis of a Novel $\mathcal{L}_1$ Adaptive Controller, Part II: Guaranteed Transient Performance. *In Proceedings of American Control Conference*, pp. 3403 - 3408, Minneapolis, MN, 2006.

[9]C. Cao and N. Hovakimyan. Guaranteed Transient Performance with $\mathcal{L}_1$ Adaptive Controller for Systems with Unknown Time-varying Parameters and Bounded Disturbances: Part I. *In Proceedings of American Control Conference*, New York, NY, 2007.

[10]C. Cao and N. Hovakimyan. Stability Margins of $\mathcal{L}_1$ Adaptive Controller: Part II. *In Proceedings of American Control Conference*, New York, NY, 2007.

[11]C. Cao and N. Hovakimyan. $\mathcal{L}_1$ Adaptive Output Feedback Controller for Systems with Time-varying Unknown Parameters and Bounded Disturbances. *In Proceedings of American Control Conference*, New York, NY, 2007.

[12]C. Cao and N. Hovakimyan. Extension of $\mathcal{L}_1$ Adaptive Output Feedback Controller to Systems of Unknown Dimension. *In Proceedings of American Control Conference*, New York, NY, 2007.

[13]M. Cao, D. Spielman, and A. Morse. A Lower Bound on Convergence of a Distributed Network Consensus Algorithm. *In Proceedings of the 44th IEEE Conference on Decision and Control*, 2005.

[14]V. Dobrokhodov, O. Yakimenko, K. Jones, I. Kaminer, I. Kitsios, and E. Bourakov. New Generation of Rapid Flight Test Prototyping System for SUAV. *In Proceedings of AIAA Modeling and Simulation Technologies Conference*, Hilton Head, SC, 2007.

[15]P. Encarnação and A. Pascoal. 3-D Path Following for Autonomous Underwater Vehicles. *In Proceedings of IEEE Conference on Decision and Control*, Sydney, Australia, 2000.

[16]P. Encarnacao, A. Pascoal, Combined trajectory tracking and path following: an application to the coordinated control of control of marine craft, IEEE Conf. Decision and Control, Orlando, Florida, 2001.

[17]M. Egerstedt and X. Hu. Formation Control with Virtual Leaders and Reduced Communications. *IEEE Transactions on Robotics and Automation*, 17(6):947-951, 2001.

[18]L. Fang, P. J. Antsaklis, and A. Tzimas, Asynchronous consensus protocols: preliminary results, simulations and open questions, 44th IEEE Conference on Decision and Control, 2005 and 2005 European Control Conference (CDC-ECC '05), pages 2194-2199, Dec. 2005.

[19]J. Fax and R. Murray. Information Flow and Cooperative Control of Vehicle Formations. *IEEE Transacions on Automatic Control*, 49(9):1465-1476, 2004.

[20]Ghabcheloo, R., A. Pedro Aguiar, Antonio Pascoal, Carlos Silvestre, Isaac Kaminer, and Joo Hespanha, "Coordinated Path-Following Control of Multiple Underactuated Autonomous Vehicles in the Presence of Communication Failures, " Proc. 45th IEEE Conference on Decision and Control (CDC), San Diego, California, USA, Dec. 13-15, 2006.

[21]Ghabcheloo, R., A. Pedro Aguiar, Antonio Pascoal, Carlos Silvestre, Isaac Kaminer, and Joo Hespanha, "Coordinated Path-Following Control of Multiple Underactuated Autonomous Vehicles in the Presence of Communication Failures, " Proc. 45th IEEE Conference on Decision and Control (CDC), San Diego, California, USA, Dec. 13-15, 2006.

[22]R. Ghabcheloo, A. Pascoal, C. Silvestre, and I. Kaminer. Nonlinear Coordinated Path Following Control of Multiple Wheeled Robots with Bidirectional Communication Constraints. *International Journal of Adaptive Control and Signal Processing*, 21:133-157, 2007.

[23]R. Ghabcheloo, A. Pascoal, C. Silvestre and I. Kaminer. Coordinated Path Following Control of Multiple Wheeled Robots Using Linearization Techniques. *International Journal of Systems Science, Taylor and Francis*, 37(6):399-414, 2006.

[24]R. Ghabcheloo, P. Aguiar, A. Pascoal, C. Silvester, I. Kaminer, J. Heshpanha. Coordinated Path-Following Control of Mobile Agents in the presence of Communcation Failues and Time-Delays, Internal report IST/ISR-NPS-UCSB Nov2006; to be submitted.

[25]C. Godsil and Royle. *Algebraic Graph Theory* Springer-Verlag, 2001.

[26]F. Giulietti, M. Innocenti, M. Napolitano and L. Pollini. Dynamics and Control Issues of Fomration Flight. *Journal of Aerospace Science and Technology*, 9:65-71, 2005.

[27]R.A. Horn and C. R. Johnson, Matrix Analysis, Cambridge University Press, 1985.

[28]A. Jadbabaie, J. Lin, and A. Morse. Coordination of Groups of Mobile Autonomous Agents Using Nearest Neighbor Rules. *IEEE Transactions on Automatic Control*, 48(6):988-1001, 2003.

[29]I. Kaminer, A. Pascoal, E. Hallberg and C. Silvestre. Trajectory Tracking for Autonomous Vehicles: An Integrated Approach to Guidance and Control. *AIAA Journal of Guidance, Control and Dynamics*, 21(1):29-38, 1998.

[30]I. Kaminer, O. Yakimenko, A. Pascoal and R. Ghabcheloo. Path Generation, Path Following and Coordinated Control for Time Critical Missions of Multiple UAVs. *In Proceedings of American Control Conference*, Minneapolis, MN, 2006.

[31]Y. Kim and M. Meshabi. On Maximizing the Second Smallest Eigenvalue of State-dependent Graph Laplacian. *IEEE Transactions on Automatic Control*, 51(1):116-120, 2006.

[32]C. Langbort, R. Chandra, and R. D'Andrea. Distributed Control of Heterogeneous Systems Interconnected Over an Arbitrary Graph. *IEEE Transactions on Automatic Control*, 9(49):1502 - 1519, 2004.

[33]L. Lapierre, D. Soetanto, A. Pascoal, Coordinated motion control of marine robots, Proc. 6th IFAC Conference on Maneuvering and Control of Marine Craft (MCMC2003), Girona, Spain, 2003.

[34]Z. Lin, B. Francis, and M. Maggiore. State Agreement for Coupled Nonlinear Systems with Time-Varying Interaction. *Submitted to SIAM Journal of Control and Optimization*, 2005.

[35]Z. Lin, B. Francis, and M. Maggiore. Necessary and Sufficient Conditions for Formation Control of Unicycles. *IEEE Transactions on Automatic Control*, 50(1):121 - 127, 2005.

[36]F. Lobo Pereira, J. Borges de Sousa, "Coordinated Control of Networked Vehicles: An Autonomous Underwater System," Automation and Remote Control, Vol. 65, No. 7, 2004, pp. 1037-1045. Translated from Avtomatika i Telemekhanika, No. 7, 2004, pp. 3-11. Original Russian Text Copyright 2004 by Pereira, Borges de Sousa.

[37]T. McLain and R. Beard, Coordination variables, Coordination Functions and Cooperative Timing Missions, *AIAA Journal of Guidance, Navigation, and Controls Conference,* vol. 28, No 1, 2005.

[38]M. Mesbahi and F. Hadaegh. Formation Flying Control of Multiple Spacecraft via Graphs, Matrix Inequalities, and Switching. *Journal of Guidance, Control and Dynamics*, 24(2):369 - 377, 2001.

[39]M. Mesbahi. On State-Dependent Dynamic Graphs and Their Controllability Properties. *IEEE Transactions on Automatic Control*, 50(3):387-392, 2005.

[40]A. Micaelli and C. Samson. Trajectory-Tracking for Unicycle -Type and Two-Steering-Wheels Mobile Robot. *Technical Report No. 2097, INRIA*, Sophia-Antipolis, France, 1993.

[41]L. Moreau, Stability of Multiagent Systems with Time - Dependent Communication Links. *IEEE Transactions on Automatic Control*, 50(2), 2005.

[42]A. Neljubov, Mathematical Methods of Air Vehicle with Thrust Vector Turn Possibility Battle, Takeoff and Landing Maneuvers Calculation. *Air Force Engineering Academy Press*, Moscow, 1986.

[43]P. Ogren, M. Egerstedt, and X. Hu. A Control Lyapunov Function Approach to Multiagent Coordination. *IEEE Transactions on Robotics and Automation*, 2002.

[44]R. Olfati-Saber and R. Murray. Agreement Problems in Networks with Directed Graphs and Switching Topology. *In Proceedings of Conference on Decision and Control*, Hawaii, USA, 2003.

[45]R. Olfati-Saber, A. Fax, and R. Murray. Consensus and Cooperation in Networked Multi-Agent Systems. *In Proceedings of the IEEE*, 95(1):1 - 17, 2007.

[46] Pascoal, A., C. Silvestre, P. Oliveira (2006). Vehicle and Mission Control of Single and Multiple Autonomous Marine Robots. In Advances in Unmanned Marine Vehicles, IEE Control Engineering Series, G. Roberts and R. Sutton (Eds).

[47] *Piccolo/Piccolo Plus autopilots - A highly integrated autopilots for small UAVs, Cloud Cap Technology, Inc., http://cloudcaptech.com/.*

[48] *J. Pomet and L. Praly, Adaptive nonlinear regulation: Estimation from the Lyapunov equation,* IEEE Trans. Autom. Contr.*, Vol. 37(6), June 1992, pp. 729–740.*

[49] *J. Pratcher, J. D'Azzo, and A. Proud. Tight Formation Control.* Journal of Guidance, Control and Dynamics*, 24(2):246 - 254, 2001.*

[50] *M. Queiroz, V. Kapila, and Q. Yan. Adaptive Nonlinear Control of Multiple Spacecraft Formation Flying.* Journal of Guidance, Control and Dynamics*, 23(3):385 - 390 , 2000.*

[51] *W. Ren, R. Beard, and T. McLain. Collective Motion and Oscillator Synchronization.* Lecture Notes in Control and Information Sciences*, Springer-Verlag, 2005.*

[52] *D. Soetanto, L. Lapierre amd A. Pascoal. Adaptive Non-Singular Path Following Control of Dynamics Wheeled Robots.* In Proceedings of ICAR*, Coimbra, Portugal, 2003.*

[53] *R. Sepulchre, D. Paley and N. Leonard. Collective Motion and Oscillator Synchronization.* In Proceedings of Block Island Workshop on Cooperative Control*, 2003.*

[54] *R. Skjetne, I. Flakstad, and T. Fossen. Formation Control by Synchronizing Multiple Maneuvering Systems.* In Proceedings of the 6th IFAC Conference on Maneuvering and Control of Marine Craft*, Girona, Spain, 2003.*

[55] *Y. Song, Y. Li, and X. Liao. Orthogonal Transformation Based Robust Adaptive Close Formation Control of Multi-UAVs.* In Proceedings of American Control Conference*, Portland, OR, 2005.*

[56] *D. Stilwell and B. Bishop.* Platoons of Underwater Vehicles. IEEE Control Systems Magazine*, pp. 45 - 52, 2000.*

[57] *D. Stilwell, E. Bollt, and D. Roberson. Sufficient Conditions for Fast Switching Synchronizations in Time-Varying Network Topologies.* SIA Journal of Applied Dynamical Systems*, 6(1):140 - 156, 2006.*

[58] *D. Stipanovic, G. Inalhan, R. Teo and C. Tomlin. Decentralized Overlapping Control of a Formation Unmanned Aerial Vehicles.* Automatica*, 40(1):1285-1296, 2004.*

[59] *H. Tanner, A. Jadbabaie, and G. Pappas. Flocking Fixed and Switching Networks.* IEEE Transactions on Automatic Control*, (to appear).*

[60] *V. Taranenko. Experience of Ritz's, Puankare's and Ljapunov's Methods Utilization for Flight Dynamics Tasks Solution.* Air Force Engineering Academy Press*, Moscow, 1986.*

[61] *V. Taranenko, and V. Momdgi. Direct Variational Method in Boundary Tasks of Flight Dynamics.* Mashinostroenie*, Moscow, 1986.*

[62] *J. Tsitsiklis and M. Athans. Convergence and Asymptotic Agreement in Distributed Decision Problems.* IEEE Transaction on Automatic Control*, 29(1), 1984.*

[63] *G. Xie and L. Wang. Consensus Control for a Class of Networks of Dynamics Agents: Fixed Topology.* In Proceedings of IEEE Conference on Decision and Conrol*, pp. 96 - 101, Seville, Spain, 2005.*

[64] *O. Yakimenko. Direct Method for Rapid Prototyping of Near-Optimal Aircraft Trajectories.* AIAA Journal of Guidance, Control, and Dynamics*, 23(5):865-875, 2000.*